The Journal of Chemical Physics ARTICLE pubs.aip.org/aip/jcp

Non-equilibrium coexistence between a fluid and a hotter or colder crystal of granular hard disks

Cite as: J. Chem. Phys. 162, 124901 (2025); doi: 10.1063/5.0250643
Submitted: 26 November 2024 • Accepted: 24 February 2025 •
Published Online: 24 March 2025

R. Maire, A. Plati, F. Smallenburg, and G. Foffi[a)]

AFFILIATIONS

Université Paris-Saclay, CNRS, Laboratoire de Physique des Solides, 91405 Orsay, France

[a)]Author to whom correspondence should be addressed: giuseppe.foffi@universite-paris-saclay.fr

ABSTRACT

Non-equilibrium phase coexistence is commonly observed in both biological and artificial systems, yet understanding it remains a significant challenge. Unlike equilibrium systems, where free energy provides a unifying framework, the absence of such a quantity in non-equilibrium settings complicates their theoretical understanding. Granular materials, driven out of equilibrium by energy dissipation during collisions, serve as an ideal platform to investigate these systems, offering insights into the parallels and distinctions between equilibrium and non-equilibrium phase behavior. For example, the coexisting dense phase is typically colder than the dilute phase, a result usually attributed to greater dissipation in denser regions. In this article, we demonstrate that this is not always the case. Using a simple numerical granular model, we show that a hot solid and a cold liquid can coexist in granular systems. This counterintuitive phenomenon arises because the collision frequency can be lower in the solid phase than in the liquid phase, consistent with equilibrium results for hard-disk systems. We further demonstrate that kinetic theory can be extended to accurately predict phase temperatures even at very high packing fractions, including within the solid phase. Our results highlight the importance of collisional dynamics and energy exchange in determining phase behavior in granular materials, offering new insights into non-equilibrium phase coexistence and the complex physics underlying granular systems.

I. INTRODUCTION

The theory of equilibrium phase coexistence as formalized by Gibbs establishes that mechanical, thermal, and chemical equilibrium are necessary conditions for the stability of a heterogeneous substance at equilibrium.[1] With the recent advancements in non-equilibrium statistical physics, it has become evident that phase coexistence phenomena are equally ubiquitous in out-of-equilibrium systems[2–4] and that Gibbs' equilibrium conditions must be relaxed, for example, in active matter systems or in driven chemical phase transitions.[4,5] This realization has sparked significant theoretical and experimental efforts to explore the differences and similarities between these non-equilibrium cases and their well-known equilibrium counterparts.[6–13] Several peculiarities characterize phase coexistence in non-equilibrium systems. For instance, in active systems, the common tangent construction fails and must be replaced by alternative constructions based on an effective free energy.[14] Similarly, the bulk density of the coexisting phases may depend on the effective surface tension,[15,16] highlighting the system's deviation from a conventional underlying free energy. Out of equilibrium, the coarsening dynamics are also unusual, with phenomena such as non-standard roughness of interfaces at coexistence,[17,18] peculiar growth of length scales during coarsening,[5,19,20] and reversed Ostwald ripening leading to bubbly phases[21,22] or microphase separation.[23] While surface tension between phases can still be defined following different equilibrium definitions, these approaches can yield different results in non-equilibrium systems.[24–27] Similarly, macroscopic heat flux between phases and peculiar interfacial properties can be observed in boundary-driven systems.[28–32] Dynamic phenomena such as traveling,[33,34] pattern-forming,[35,36] and even chasing coexisting phases[37] have been observed as well.

Recently, inspired by biologically active systems, a growing interest in underdamped self-propelled particles surfaced.[38–41]

Among other things, it has been observed that these particles can undergo a motility-induced phase separation,[42–44] with a dense phase colder[45] than the dilute one due to reduced effective self-propulsion in the dense phase.[5] This highly non-equilibrium effect was recently observed in an experimental system.[46] In contrast, Ref. 47 reported motility-induced phase separation resulting in a hotter solid. Similar observations, in stark contrast to Gibbs' requirement of thermal equilibrium, were previously made in the study of vibrated granular media, where gas–liquid[48–59] and liquid–solid phase coexistence[60–70] consistently revealed a colder dense phase. These results have traditionally been explained by the assumption that the denser phase must dissipate more energy and, therefore, be colder due to a higher collision frequency compared to the coexisting dilute phase.

Nonetheless, a hotter solid was recently observed in a driven 2D granular system.[71] This phenomenon was, however, attributed to boundary effects rather than induced by the inter-particle interaction. In a recent realistic numerical study of a vibrated quasi-2D granular system, we also surprisingly observed that a crystal composed of bidisperse beads can exhibit a hotter solid than the coexisting liquid.[72] This temperature difference partially arose from geometric effects that cannot occur in a monodisperse system. In this paper, we simplify the previously used model by employing only monodisperse beads and demonstrate that even for such simple systems, it is possible to find a solid phase hotter than the coexisting liquid. Surprisingly, we find that dissipation during collisions can be the key mechanism for a hotter solid. By developing a kinetic theory to explain these results, we show that, although the solid phase is always denser, its particle collision frequency is typically lower than in the coexisting liquid, reducing dissipation and enabling the solid to be hotter.

This paper is organized as follows: in Sec. II, we present and simulate a simple 2D granular model in the liquid–solid coexistence region, showing how a hotter solid can emerge. In Sec. III, we explain this behavior using an equilibrium-like argument based on the collision frequency of hard-disk coexisting phases and then extend the discussion with a fully non-equilibrium theory. Finally, in Sec. IV, we discuss the relevance and broader implications of our findings.

II. NUMERICAL INVESTIGATIONS

To explore the temperature differences between the coexisting liquid and solid phases in a system of dissipative hard disks, we consider a simple model system with two distinct limits. In this section, we describe both the model and the simulation methods we use to study them.

A. The model

A quasi-2D vibrated box serves as a paradigmatic system for investigating driven granular systems.[52,63,67,73–80] In this setup, particles are confined within a quasi-2D horizontal plane, bounded by parallel top and bottom plates. The system is driven by vertical vibrations of the container, which inject energy into the vertical degrees of freedom of the particles. This energy is subsequently dissipated and redistributed across the horizontal plane through inter-particle collisions.

To capture the essential physics of the quasi-2D system, we propose the following 2D coarse-grained model. The system is made of 2D dissipative hard disks of mass m and diameter σ. When two particles collide, they can both dissipate energy and gain momentum, leading to the following collision rule:[73,81]

$$\begin{aligned} \boldsymbol{v}_i' &= \boldsymbol{v}_i - \left[\frac{1+\alpha}{2}(\boldsymbol{v}_{ij}\cdot\hat{\boldsymbol{\sigma}}_{ij}) + \Delta\right]\hat{\boldsymbol{\sigma}}_{ij}, \\ \boldsymbol{v}_j' &= \boldsymbol{v}_j + \left[\frac{1+\alpha}{2}(\boldsymbol{v}_{ij}\cdot\hat{\boldsymbol{\sigma}}_{ij}) + \Delta\right]\hat{\boldsymbol{\sigma}}_{ij}, \end{aligned} \tag{1}$$

where $\boldsymbol{v}_i'$ is the post-collisional velocity of particle i, while $\hat{\boldsymbol{\sigma}}_{ij}$ and $\boldsymbol{v}_{ij}$ are, respectively, the unit vector joining particles i and j and the relative velocity between them. The coefficient of restitution $0 < \alpha < 1$ governs the dissipation during collisions, and $\Delta > 0$ is responsible for the velocity injection. This velocity injection mimics the energy redistribution during grain–grain collisions in the quasi-2D system described above. The energy change during a collision can be either positive or negative, depending on the relative velocity of the particles. For large relative velocities, $|\boldsymbol{v}_{ij}| \gg \Delta$, and sufficiently small α, the term proportional to α dominates, leading to dissipative collisions. Conversely, at low relative velocities, energy dissipation through α is minimal, and instead, particles gain an additional velocity Δ, effectively injecting energy into the system.

Between collisions, the hard disks are also coupled to an external bath at granular temperature T_b with drag γ via a Langevin equation,

$$\frac{\mathrm{d}\boldsymbol{v}}{\mathrm{d}t} = -\gamma\boldsymbol{v} + \sqrt{2\gamma T_b/m}\,\boldsymbol{\eta}, \tag{2}$$

where $\boldsymbol{\eta}$ is a random vectorial white Gaussian noise with unit variance and zero mean. Comparing again to a vibrated quasi-2D granular system, this effective noise would represent the roughness of the top and bottom plates confining the particles in the realistic quasi-2D model. Collisions with these plates cause the hard disks to behave as Brownian particles on the horizontal plane for time scales larger than the one set by the frequency of the shaking.[82,83]

We focus on two limiting cases of interest:

- The *$\Delta+\gamma$ model*, where $T_b = 0$.[73,84] Here, particles lose energy during their free flight according to $v(t) = v_0 e^{-\gamma t}$, while collisions, on average, increase the system's energy—although in some cases, they may also lead to energy loss. This 2D model is representative of a quasi-2D system in a dynamical regime where particles are shaken with sufficient energy to undergo strong collisions with both the lower and the upper plate. γ effectively accounts for the horizontal energy loss due to tangential friction with the smooth plates, while Δ reproduces the energy transfer between the vertical and horizontal degrees of freedom at collision. The equilibrium limit corresponds to $\Delta \to 0$, $\alpha \to 1$, and $\gamma \to 0$.
- The *granular Langevin model* (GLM), where $\Delta = 0$.[72,82] In this case, all the energy is supplied by the bath, and collisions only dissipate energy. In the quasi-2D system, this corresponds to grains confined between rough plates that are not strongly shaken, which limits their vertical motion

and interaction with the upper plate. In this regime, surface asperities transfer energy primarily into the horizontal plane during grain–plate collisions, while grain–grain collisions contribute minimally to the energy change in the horizontal plane. In the limit $\alpha \to 1$, we recover an equilibrium system.

B. Numerical simulations

Using event-driven molecular dynamics,[89] we simulate both models described above using up to $N \simeq 10^5$ particles in boxes of size $L_x \times L_y$ with periodic boundary conditions. We define $\phi = N\pi(\sigma/2)^2/L_xL_y$ as the packing fraction of the system and focus on the region near the equilibrium liquid–hexatic transition. For simplicity, we will refer to the crystalline or hexatic phase in coexistence with the liquid as the "solid phase" of the system without making a distinction between the two.

The granular temperature T of the system is defined as[90,91]

$$T = \frac{1}{2}m\sum_{i=1}^{N}\langle \boldsymbol{v}_i^2\rangle, \tag{3}$$

where $\langle\cdots\rangle$ represents a time average. When explicitly stated, it also includes an average over different initial conditions. In addition, we define the pressure p as the virial pressure (see Appendix A),

$$p = \frac{NT}{L_xL_y} + \frac{m\sigma}{2L_xL_yt}\sum_{\text{coll}-ij}\left(\frac{1+\alpha}{2}(\boldsymbol{v}_{ij}\cdot\hat{\boldsymbol{\sigma}}_{ij}) + \Delta\right). \tag{4}$$

We present the results of our simulations in the coexistence region of the liquid–solid phase transition in Fig. 1. The top panels show the results for the $\Delta + \gamma$ model, while the bottom panels display the results for the GLM. For the $\Delta + \gamma$ model, we observe a Mayer–Wood loop[85,92,93] in the pressure [panel (a)], indicating a first-order phase transition. More intriguingly, in the coexistence region, the granular temperature also exhibits a non-monotonic trend [panel (b)]. Unlike the loop in pressure, this phenomenon is not related to interfacial effects, as it does not disappear with increasing N. Instead, it is most likely associated with the coexistence of two phases at different temperatures. Indeed, if the existence of a lever-rule for the density field is assumed,[72] the temperature field, which is slaved to the density and crystallization field, should also follow a lever-rule. As the density increases, a larger fraction of the system transitions to the solid phase, following the conventional lever-rule for the density field. Consequently, a greater portion of the system attains the temperature of the solid. Since in panel (b) the global temperature decreases, we hypothesize that the coexisting solid phase is colder than the coexisting liquid phase. This is confirmed by direct computations of the temperature $T(x)$ and density $\phi(x)$ profiles, corresponding to a given phase separation, averaged over multiple

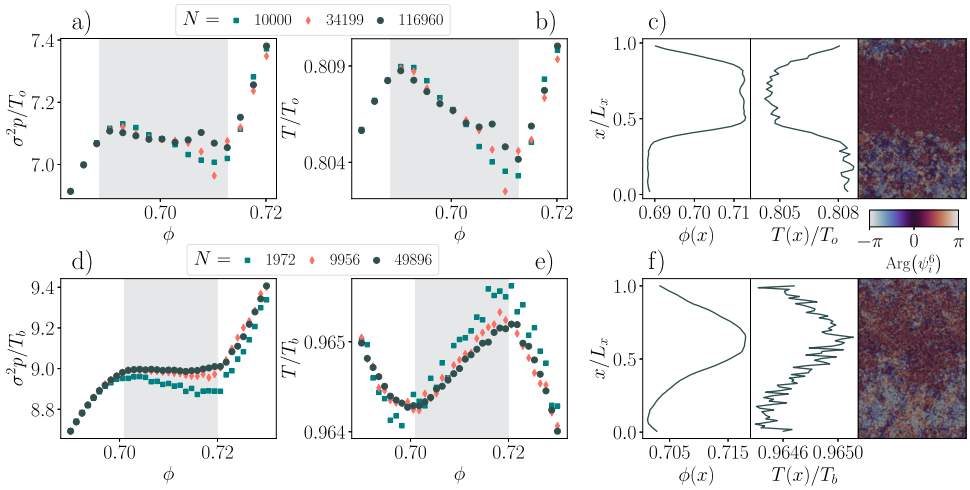

FIG. 1. Top: $\Delta + \gamma$ model ($\Delta/\sigma\gamma = 1.1$ and $\alpha = 0.95$), and bottom: GLM [$T_b/m(\sigma\gamma)^2 = 0.125$ and $\alpha = 0.99$]. (a) and (d) Pressure as a function of the density. (b) and (e) Energy as a function of the density. First two panels of (c) and (f) show granular temperature and density averaged over a y slab in $[x, x + 10\sigma]$. Last panel of (c) and (f) shows snapshot of a liquid–solid coexistence, particles are colored by the angle of hexatic local order parameter $\mathrm{Arg}(\psi_i^6)$ with $\psi_i^6 = \sum_{j=1}^{N_i} e^{i6\theta_{ij}}/N_i$, where N_i is the number of neighbors to particle i and θ_{ij} is the angle in real space between i and j. The density and temperature profiles in (c) represent the time-averaged values over 2×10^4 measurements of the properties obtained from the time evolution of the displayed snapshot. The measurement window is sufficiently small to ensure that large variations in the density field remain negligible. The coexistence behavior of the GLM is more challenging to visualize compared to that of the $\Delta + \gamma$ model. This difficulty arises because its behavior closely mirrors the equilibrium liquid–hexatic phase coexistence, where the transition between the two phases is extremely weak, resulting in strongly fluctuating interfaces.[85] For this system, the profiles are obtained by averaging 10^5 snapshots over 60 independent realizations. Before performing the averaging, all particles are shifted such that the center of mass[86] is positioned at $x/L_x = 0.75$, ensuring that the solid phase consistently resides in the region $0.5 < x/L_x < 1$.[87,88] Therefore, unlike in the $\Delta + \gamma$ model, the snapshot of the GLM in (f) does not correspond to the ones used to extract the profiles. Note finally that for the $\Delta + \gamma$ model, the lack of a thermal bath means there is no obvious external reference temperature to compare the measured T to. Hence, for this system, we plot the temperature in terms of T_o, which we define as the theoretical temperature of the Delta model assuming velocity distributed as a Gaussian and in the absence of drag ($\gamma = 0$). It is given by Ref. 81 $T_o = \frac{1}{2}m\Delta^2\left(\alpha\sqrt{\pi}/2 + \sqrt{\alpha^2\pi/4 + (1-\alpha)^2}\right)^2/(1-\alpha^2)^2$ and is independent on the density.

realizations and snapshots [panel (c)]. For the GLM, the pressure loop is still evident [panel (d)], indicating a first-order phase transition. The temperature also presents the expected non-monotonic trend [panel (e)], but in this case, the solid is hotter than the liquid, as the global temperature increases. This observation is corroborated by direct computations of the local temperature and densities [panel (f)].

Therefore, we find a solid that is hotter than the liquid in the GLM, even though the collisions are purely dissipative. Surprisingly, in the $\Delta + \gamma$ model, where energy is injected during collisions, the solid is colder.

Before delving into the theory explaining these intriguing results, we note that, both for the GLM and the $\Delta + \gamma$ model, the energy difference between the two phases is rather low (i.e., between 0.1% and 0.3%). This rather small temperature difference ultimately stems from the small density difference between the liquid and the solid, as well as our choice of parameters, which keeps the system relatively close to equilibrium. Maintaining this proximity to equilibrium is essential for the validity of the theoretical framework we will develop. In addition, we point out that in the GLM, further increasing dissipation readily leads to a continuous phase transition and the disappearance of the phase coexistence. This phenomenon is discussed in greater detail in Appendix B.

III. THEORY

A. Equilibrium argument for the temperature difference

In order to gain intuition about the surprising results concerning the temperature of both phases, we provide an intuitive argument grounded on an equilibrium description. Assuming the system remains close to equilibrium, we will for now utilize equilibrium results for the pressure to infer the possible temperature difference between the two phases that are slightly out of equilibrium.

Consider a coexistence between a liquid and a solid of hard disks *at equilibrium*. For hard disks, the pressure can be directly related to the contact value g^+ of the pair correlation function,[94]

$$p^{eq}(\phi, T, \phi g^+) = \frac{4\phi}{\sigma^2 \pi} T(1 + 2\phi g^+). \tag{5}$$

Note that even in equilibrium, we still define T as the average kinetic energy of a particle [see Eq. (3)]. The constraint of mechanical equilibrium between the solid and the liquid phase can, therefore, be written as

$$\phi_s T(1 + 2\phi_s g_s^+) = \phi_l T(1 + 2\phi_l g_l^+), \tag{6}$$

where g_s^+ and g_l^+ are the equilibrium pair correlation functions at contact in the solid and in the liquid, respectively. Note that the temperature T is the same for both phases, as we are considering an equilibrium system. Since $\phi_s > \phi_l$, it follows from Eq. (6) that

$$\phi_s g_s^+ < \phi_l g_l^+. \tag{7}$$

Moreover, the pressure of a hard-disk system is directly connected to the rate of collisions,[94] leading to the Enskog expression for the collision frequency ω,[95]

$$\omega(T, \phi g^+) = 8\phi g^+ \sqrt{T/\sigma^2 \pi m}, \tag{8}$$

which holds exactly in equilibrium. We will later check the validity of this assumption, especially in the solid. This implies from Eqs. (7) and (8) that the collision frequency in the solid is lower than in the liquid at coexistence,

$$\omega(T, \phi_s g_s^+) < \omega(T, \phi_l g_l^+). \tag{9}$$

In other words, the increase in density in the solid is compensated by a decrease in the collision frequency, such that the momentum exchange rate—or equivalently, the pressure—remains the same in both the liquid and the solid phases. We now assume that close to equilibrium, the collision frequency in the coexisting liquid is still higher than in the solid. Under this approximation, in systems where energy is dissipated during collisions, the liquid phase is expected to be colder than in the coexisting solid. The same argument suggests a higher temperature in the coexisting liquid than in the solid when energy is injected during collisions. However, outside the coexistence region, the collision rate increases monotonically with density, causing the temperature to decrease with density for dissipative collisions and increase when energy is injected at collision. This contrast between inside and outside the coexistence region explains the non-monotonic trend of the energy in both models shown in Fig. 1.

In this argument, we assumed that the non-equilibrium systems we consider here can be regarded as small perturbations to an equilibrium system, such that g^+ and the temperature of the system are only weakly affected by the introduction of non-equilibrium effects. Although this equilibrium picture provides an intuitive argument for the expected behavior of the temperature difference, it leads to an internal inconsistency, where we use the assumption of thermal equilibrium to show the emergence of a temperature difference. In Sec. III B, we explicitly take the temperature difference between the two phases into account in our analysis to derive it in a consistent way.

B. Non-equilibrium derivation of the temperature difference

We now take into account the non-equilibrium nature of our system. Assuming that velocities follow a Gaussian distribution and are uncorrelated before collisions, we find that the pressure p in either phase can be written as (see Appendix A)

$$p(\phi, T, \phi g^+) = \frac{4\phi}{\sigma^2 \pi}\left[T + \phi g^+\left((1+\alpha)T + 2\Delta\sqrt{\pi m T}\right)\right], \tag{10}$$

where we still find the ideal contribution and the virial contribution proportional to $(1+\alpha)T$, which represents momentum redistribution due to particle interactions. A new term proportional to Δ emerges from non-equilibrium velocity injection during collisions.[96]

The steady state temperature arises from a balance between dissipation and energy injection.[81] Under the same assumptions as for the pressure, it can be shown that (see Appendix C)

$$\frac{\omega(T, \phi g^+)}{2}\left(m\Delta^2 + \alpha\Delta\sqrt{\pi m T} - (1-\alpha^2)T\right) - 2\gamma(T - T_b) = 0. \tag{11}$$

The first term of Eq. (11) represents the rate of energy change due to collisions, with the expression in parentheses describing the average energy change per collision. The second term accounts for energy

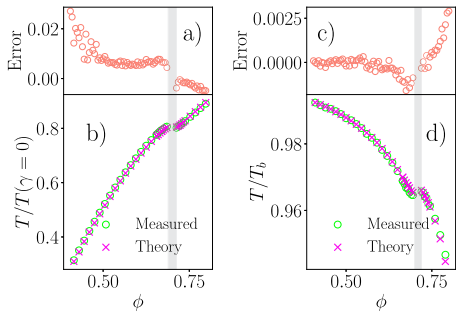

FIG. 2. Comparison between kinetic theory predictions and measured values of temperature. Panels (a) and (b) show the temperature predicted by kinetic theory (using measured values of g^+) compared to the directly measured temperature for the $\Delta + \gamma$ model. The error is calculated as $(T_{\text{measured}} - T_{\text{theory}})/T_{\text{theory}}$. Panels (c) and (d) present the same comparison for the GLM. Both models are simulated utilizing the same parameters as in Fig. 1.

exchange with the thermal bath. A crucial consequence of Eq. (11) is that the temperature depends on the density only through the frequency of collision. Therefore (far from the solid–liquid interface and when $\gamma \neq 0$), the temperatures of the coexisting phases can be assumed to depend solely on their respective values of ϕg^+.

This approach assumes that the velocity distribution remains approximately Gaussian and that velocities are uncorrelated during collisions. Together, these assumptions lead directly to Enskog's formula for the collision frequency [Eq. (8)], which we apply here. However, since we are interested in dense fluids and solids that, in principle, lie beyond the domain where Enskog theory applies, it is essential to test these assumptions. To this end, in Figs. 2(a) and 2(c), we compare measured temperatures to theoretical predictions for both the $\Delta + \gamma$ model and the GLM, respectively. These predictions were obtained using direct measurements of g^+ and the numerically calculated root of Eq. (11). Overall, the theory agrees well with numerical data, as demonstrated by the errors; see Figs. 2(b) and 2(d). Notably, for the $\Delta + \gamma$ model, the theory underperforms in the dilute limit due to an absorbing phase transition near $\phi \simeq 0.25$, where molecular chaos significantly breaks down.[73,97] In contrast, the GLM behaves as expected: the theory is accurate at low densities but becomes less reliable as the packing fraction is increased. It may seem surprising that Enskog's theory, often considered valid only in the dilute limit, performs well here, even under non-equilibrium steady states. For instance, the theory is known to inaccurately predict transport coefficients, such as viscosity, in dense fluids,[98] as these predictions are highly sensitive to collective effects and long-time tails[98] that Enskog's framework cannot capture. However, quantities such as the collision frequency that depend solely on the local environment are less affected by these non-local features. Based on these results, we conclude that the kinetic theory can be trusted to accurately predict temperatures within the parameter region studied $(\alpha > 0.95)$.

The results presented in Fig. 2 show that the theory predicts well the non-monotonicity of the temperature. However, it requires measuring the values of g^+. While equilibrium predictions[98] proved to be good approximations for driven dissipative systems,[73,99–101] we will demonstrate that we can make useful predictions about the temperatures of both phases in the coexistence region of non-equilibrium hard disk systems without resorting to this approximation or relying on any equation of state.

Having tested the validity of our approximations as a first step, we note that mechanical stability still requires the equality of pressure of both phases,

$$p(\phi_s, T_s, \phi_s g_s^+) = p(\phi_l, T_l, \phi_l g_l^+). \tag{12}$$

For simplicity, we assumed flat interfaces between the phases, avoiding the need to account for Laplace pressure and other interfacial stresses,[102] which could influence the temperatures of each phase. The key insight is that energy change at collision implies that the density dependence of energy arises solely from the collision frequency, which in the Enskog approximation depends on density only through ϕg^+ [Eq. (8)]. This means that ϕg^+ can be found if the temperature is known. Indeed, we can isolate ϕg^+ in the equation for the temperature Eq. (11) by inserting ω defined in Eq. (8) into it,

$$\phi g^+ \equiv \mathcal{G}(T) = \frac{\sigma\gamma\sqrt{\pi m}(T - T_b)}{2\sqrt{T}(m\Delta^2 + \alpha\Delta\sqrt{\pi m T} - (1-\alpha^2)T)}. \tag{13}$$

This allows us to eliminate the dependence on ϕg^+ in the pressure Eq. (12),

$$p(\phi_s, T_s, \mathcal{G}(T_s)) = p(\phi_l, T_l, \mathcal{G}(T_l)). \tag{14}$$

By eliminating ϕg^+, the pressure now explicitly depends only linearly on the density,

$$p(\phi, T, \mathcal{G}(T)) = \phi\tilde{p}(T, \mathcal{G}(T)), \tag{15}$$

where $\tilde{p}$ is defined as

$$\tilde{p}(T, \mathcal{G}(T)) = \frac{\sigma^2\pi}{4}\frac{p}{\phi}, \tag{16}$$

which does not depend on ϕ. Finally, using mechanical equilibrium [see Eq. (14)] between phases and $\phi_s > \phi_l$, we find a non-equilibrium criterion,

$$\tilde{p}(T_s, \mathcal{G}(T_s)) < \tilde{p}(T_l, \mathcal{G}(T_l)). \tag{17}$$

Equation (17) allows us to determine which phase is hotter based on $\mathcal{G}$, without needing to know an equation of state or g^+. For instance, if $\tilde{p}(T)$ is a continuous and increasing function of T, then Eq. (17) implies $T_s < T_l$. However, if $\tilde{p}$ is non-monotonic, the temperature comparison becomes more complex.

C. Hotter or colder solid?

We first focus on the $\Delta + \gamma$ model $(T_b = 0)$. In this model, $\tilde{p}$ is a continuous and monotonically increasing function of the physically accessible granular temperatures (see Appendix D). Consequently, from Eq. (17), we find that

$$T_s^{\Delta+\gamma} < T_l^{\Delta+\gamma}. \tag{18}$$

As confirmed by our simulations, the temperature of the solid is predicted to be lower than that of the liquid, regardless of the parameters $\Delta > 0$ and $\gamma > 0$. Note that this theory still assumes molecular

chaos and a Gaussian velocity distribution; therefore, it should only be trusted near equilibrium conditions.

The theory for the GLM ($\Delta = 0$) is more intricate than that of the $\Delta + \gamma$ model. For this model, we obtain (see Appendix E)

$$\tilde{p}^{\mathrm{GLM}}(\tilde{T}) = T_b \tilde{T}\left(1 + \Lambda(1-\tilde{T})\tilde{T}^{-3/2}\right), \tag{19}$$

with

$$\tilde{T} = T/T_b \quad \text{and} \quad \Lambda = \frac{\gamma\sigma\sqrt{\pi m/T_b}}{2(1-\alpha)} > 0. \tag{20}$$

Λ is a dimensionless parameter such that, at the Gaussian level, $\Lambda \to \infty$ corresponds to the equilibrium limit. Since the thermal bath is the only source of energy injection, the physical temperatures are constrained by $\tilde{T} < 1$.

For $\Lambda > 1$, $\tilde{p}$ is continuous and decreasing for $\tilde{T} < 1$, leading to the result

$$T_l^{\mathrm{GLM}} < T_s^{\mathrm{GLM}} \text{ when } \Lambda > 1. \tag{21}$$

This explains the outcome observed in Fig. 1, where the solid was found to be hotter than the liquid in the GLM (with $\Lambda \simeq 10^2$).

However, in the strongly non-equilibrium case where $\Lambda < 1$, unlike the $\Delta + \gamma$ model, $\tilde{p}$ is not monotonically increasing, complicating the analysis. Nevertheless, we saw in Appendix B that for these small Λ, the liquid–solid transition was most likely always continuous (i.e., without phase coexistence).

IV. DISCUSSION

Our investigations have shown that, in a granular system, the solid phase in a solid–liquid coexistence can indeed be hotter than the liquid. A heuristic, equilibrium-based argument for this counterintuitive result is that, at coexistence, the collision frequency in the solid phase is lower than in the liquid phase. Therefore, in systems where energy is dissipated through collisions, it is natural to expect the solid to be hotter than the liquid, even if the former is denser than the latter.

Although these heuristic arguments provide an intuitive explanation for our findings, they start from an equilibrium assumption, with constant temperature throughout the system, rendering them inconsistent when used to predict temperature differences. The more rigorous analysis in Sec. III overcomes this limitation by explicitly incorporating the temperature difference between the two phases.

In developing the theory, we made certain assumptions that may not strictly hold out of equilibrium. In particular, we assumed molecular chaos and a Gaussian velocity distribution, which can easily break down,[96,103–106] particularly in the solid phase. However, we show that close to equilibrium, the predictions from kinetic theory work exceptionally well even in the solid. We also showed in Ref. 72 that the theory still works even in a binary mixture where energy equipartition between small and large disks does not hold. Extensions beyond the Gaussian assumption are possible[96,103,107,108] but fall outside the scope of this article.

The models we introduced are simplified compared to realistic granular experiments, such as quasi-2D vibrated granular matter. As a first step, the analysis performed on the two limiting models can be extended to the full system with $\Delta \neq 0$ and $T_b \neq 0$. However, nothing too surprising emerges from this extension: either the bath or Δ dominates the energy injection, and the temperature difference follows. In more realistic systems of quasi-2D vibrated monodisperse granular beads, the dense phase was always found to be colder than the dilute one due to effects not accounted for in our simplified 2D model: bistability of the grain–plate dynamics,[67,109] strong vertical confinement,[63] dynamical instabilities,[48,50] and non-homogeneous energy injection,[58] among others. While our study has the merit of showing that the temperature difference commonly observed in granular systems cannot be solely explained by dissipative collision, a crucial next step would be to incorporate these factors into our model to gain a better understanding of what governs the temperature difference between the two phases. Conversely, from an experimental standpoint, it would be interesting to optimize the realistic parameters of the quasi-2D system to get as close as possible to the effective GLM and to investigate whether it is feasible to obtain a monodisperse granular solid that is hotter than its coexisting liquid. We also note that in multi-component hard disk mixtures, where a variety of crystal and quasi-crystal structures can form,[74,110–112] a granular solid was observed to be hotter than the liquid in a realistic quasi-2D vibrated system. This is because collisions between some species are geometrically impossible in a perfect crystal but not in the liquid, reducing a source of dissipation only in the dense phase.[72]

In active matter, motility-induced phase separation can be realized by self-propelled macroscopic agents undergoing dissipative collisions.[6,46] Since the phase separation in these systems arises from a dynamical instability associated with a reduction in effective self-propulsion—and, consequently, in effective temperature—as the system's density increases, it is unlikely that the effect we have identified plays a significant role in these cases.

In addition, our theory assumes the solid–liquid transition is discontinuous. However, for the GLM, we found that this is not always the case (see Appendix B). This could be attributed to the softening of the effective interaction due to dissipative collisions.[113–115] Indeed, particles with potentials softer than hard-core repulsion are known to undergo the standard two-step Kosterlitz–Thouless–Halperin–Nelson–Young (KTHNY) melting transition[116–120] from a solid to a hexatic and then from a hexatic to a liquid phase, which both occur continuously.[121,122] Finally, the question of hexatic order in these systems is of significant interest and was not addressed in this study. Recent work has shown that crystals formed in the $\Delta + \gamma$ model exhibit translational long-range order due to hyperuniformity,[84,123–125] in striking violation of the Mermin–Wagner theorem. It would be interesting to explore the impact of temperature difference and translational long-range order on the nature of the melting of granular crystals.

ACKNOWLEDGMENTS

A.P. acknowledges the Agence Nationale de la Recherche (ANR), Grant No. ANR-21-CE06-0039, which provided the funding for this research.

AUTHOR DECLARATIONS

Conflict of Interest

The authors have no conflicts to disclose.

Author Contributions

R. Maire: Conceptualization (lead); Data curation (lead); Formal analysis (lead); Investigation (lead); Methodology (lead); Writing – original draft (lead); Writing – review & editing (equal). **A. Plati**: Conceptualization (lead); Formal analysis (lead); Investigation (lead); Writing – original draft (supporting); Writing – review & editing (equal). **F. Smallenburg**: Conceptualization (supporting); Formal analysis (supporting); Project administration (lead); Supervision (lead); Writing – original draft (supporting); Writing – review & editing (supporting). **G. Foffi**: Conceptualization (equal); Formal analysis (equal); Project administration (lead); Supervision (lead); Writing – original draft (equal); Writing – review & editing (equal).

DATA AVAILABILITY

The data that support the findings of this study are available from the corresponding author upon reasonable request.

APPENDIX A: DETERMINATION OF THE PRESSURE

The typical method for obtaining the pressure at equilibrium is through the virial pressure formula. Out of equilibrium, pressure can either be derived from the Boltzmann equation or through a method analogous to that used in equilibrium. In this work, we follow the latter approach. The pressure p in 2D systems interacting through two-body forces can be written as[126]

$$p = \frac{4\phi}{\sigma^2\pi}\left(T - \frac{1}{2N}\sum_{i<j}^{N}\langle \boldsymbol{r}_{ij}\cdot\boldsymbol{F}_{ij}\rangle\right), \tag{A1}$$

where $\boldsymbol{F}_{ij}$ is the force between particles i and j. Similar to equilibrium systems, the Langevin thermostat only contributes to the ideal part of the pressure and does not affect the virial term, which arises from momentum exchanges between particles. Notably, Eq. (A1) can also be derived from a direct evaluation of the momentum exchange at a boundary.

The force between particles i and j can be derived from the collision rule Eq. (1) using $m\mathrm{d}\boldsymbol{v}_i/\mathrm{d}t = \boldsymbol{F}_{ij}$,

$$\boldsymbol{F}_{ij} = -m\left(\frac{1+\alpha}{2}|\boldsymbol{v}_{ij}\cdot\hat{\boldsymbol{\sigma}}_{ij}| + \Delta\right)\hat{\boldsymbol{\sigma}}_{ij}\delta(t - t_{ij}^{\mathrm{coll}}), \tag{A2}$$

with t_{ij}^{coll} being the time of collision between particle i and j. Equation (A1) can be simplified using Enskog's collision frequency (C6), the expression of the instantaneous force (A2), and the collisional average defined in Eq. (C5),

$$\begin{aligned} p &= \frac{4\phi}{\sigma^2\pi}\left[T + \frac{m\sigma\omega(T,\phi g^+)}{4}\left\langle\frac{1+\alpha}{2}|\boldsymbol{v}_{ij}\cdot\hat{\boldsymbol{\sigma}}_{ij}| + \Delta\right\rangle_{\mathrm{coll}}\right] \\ &= \frac{4\phi}{\sigma^2\pi}\left[T + \phi g^+\sqrt{T}\left((1+\alpha)\sqrt{T} + 2\sqrt{\pi m}\Delta\right)\right], \end{aligned} \tag{A3}$$

which coincides with Eq. (10) in the main text.

Note that from the average we can also obtain an expression for the microscopic running pressure used in the event-driven simulations to measure the pressure,

$$p_{\mathrm{micro}} = \frac{NT}{L_xL_y} + \frac{m\sigma}{2L_xL_yt}\sum_{\mathrm{coll-ij}}\left(\frac{1+\alpha}{2}(\boldsymbol{v}_{ij}\cdot\hat{\boldsymbol{\sigma}}_{ij}) + \Delta\right), \tag{A4}$$

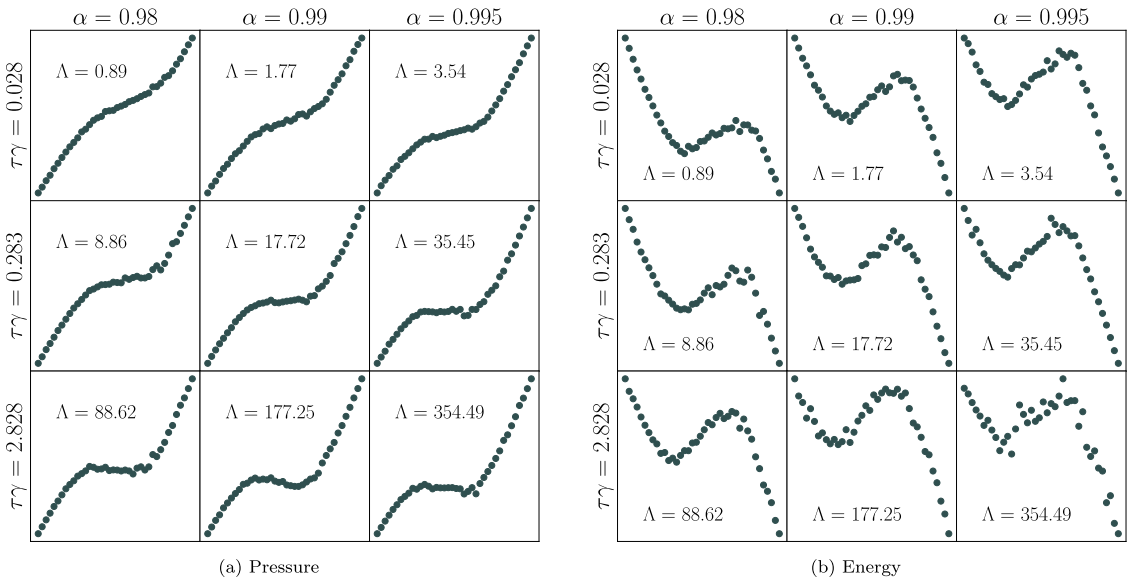

FIG. 3. (a) Evolution of pressure (in arbitrary units) as a function of density for the GLM, for various γ and α ($\tau = \sqrt{m\sigma^2/T_b}$). (b) Same as shown in (a), but for the energy instead of the pressure (in arbitrary units). $N = 10^4$.

where t is the time simulation window and the sum is over all collisions.

APPENDIX B: FROM DISCONTINUOUS TO CONTINUOUS LIQUID–SOLID PHASE TRANSITION

The liquid–solid phase transition in the GLM can become continuous under certain conditions. In the equilibrium limit $\Lambda \to \infty$, the model appears to transition from the liquid to the solid phase (most likely a hexatic phase) in a discontinuous manner, as shown in Fig. 3(a). This is consistent with the known behavior of equilibrium hard-disks.[85] However, as Λ decreases and dissipation becomes more significant, the transition appears to become continuous, with no Mayer–Wood loop[92]—indicative of strong, finite-sized interfacial effects—observed in the pressure. This behavior is reminiscent of the classical two-step Kosterlitz–Thouless–Halperin–Nelson–Young (KTHNY) transition, where the liquid-to-hexatic transition is continuous. It has been shown that systems interacting with soft potentials—for example, $V(r) \propto r^n$ with $n < 6$—can follow the KTHNY scenario in transitioning from the solid to the liquid phase.[121,122]

In our system, the observed change in behavior as dissipation increases may be explained by an effective softening of the hard-disk potential.[113–115] However, further studies are necessary to fully understand the mechanisms underlying this change in the nature of the transition.

Interestingly, a loop in the energy is consistently observed in Fig. 3(b), regardless of whether the transition is continuous or discontinuous. This suggests that even in the absence of a first-order phase transition, the structural changes associated with the transition to the solid phase lead to an increase in temperature around the transition point.

We finally note that a change from continuous to discontinuous in the liquid–solid transition was also observed in an experimental vibrated granular gas in Refs. 75 and 76 upon changing driving parameters and in Ref. 60 while changing the properties of the grains.

APPENDIX C: DETERMINATION OF THE TEMPERATURE

We define the instantaneous energy of the system as $E = m/2\sum_{i=1}^{N} \boldsymbol{v}_i^2$. From the collision rule, the energy change during a collision is given by

$$\Delta E = m\Delta^2 + \alpha m(\boldsymbol{v}_{ij}\cdot\hat{\boldsymbol{\sigma}}_{ij})\Delta - m\frac{1-\alpha^2}{4}(\boldsymbol{v}_{ij}\cdot\hat{\boldsymbol{\sigma}}_{ij})^2. \tag{C1}$$

The evolution of the temperature in the system is then given by

$$\frac{\mathrm{d}T}{\mathrm{d}t} = \frac{\omega}{2}\langle\Delta E\rangle_{\mathrm{coll}} - 2\gamma(T - T_b), \tag{C2}$$

where ω is the collision frequency and $\langle\cdots\rangle_{\mathrm{coll}}$ is an average over collisions defined from the Boltzmann equation as

$$\langle A(\boldsymbol{v}_{ij},\hat{\boldsymbol{\sigma}}_{ij})\rangle_{\mathrm{coll}} = \frac{\int d\boldsymbol{v}_i \int d\boldsymbol{v}_j \int d\hat{\boldsymbol{\sigma}}_{ij}\Theta(-\boldsymbol{v}_{ij}\cdot\hat{\boldsymbol{\sigma}}_{ij})|\boldsymbol{v}_{ij}\cdot\hat{\boldsymbol{\sigma}}_{ij}|A(\boldsymbol{v}_{ij},\hat{\boldsymbol{\sigma}}_{ij})f^{(2)}(\boldsymbol{v}_i,\boldsymbol{v}_j,\hat{\boldsymbol{\sigma}}_{ij})}{\int d\boldsymbol{v}_i \int d\boldsymbol{v}_j \int d\hat{\boldsymbol{\sigma}}_{ij}\Theta(-\boldsymbol{v}_{ij}\cdot\hat{\boldsymbol{\sigma}}_{ij})|\boldsymbol{v}_{ij}\cdot\hat{\boldsymbol{\sigma}}_{ij}|f^{(2)}(\boldsymbol{v}_i,\boldsymbol{v}_j,\hat{\boldsymbol{\sigma}}_{ij})}. \tag{C3}$$

Θ is the Heaviside function that ensures only particles approaching each other are considered, $|\boldsymbol{v}_{ij}\cdot\hat{\boldsymbol{\sigma}}_{ij}|$ can be interpreted as a flux time a cross section for the hard-disk interaction, and $f^{(2)}(\boldsymbol{v}_1,\boldsymbol{v}_2,\boldsymbol{\sigma}_{ij})$ is the pair distribution function of the velocities. Assuming molecular chaos with Enskog's extension, we simplify the two point velocity distribution,

$$f^{(2)}(\boldsymbol{v}_i,\boldsymbol{v}_j,\hat{\boldsymbol{\sigma}}_{ij}) \simeq g^+ f(\boldsymbol{v}_i)f(\boldsymbol{v}_j), \tag{C4}$$

where g^+ is the pair correlation function at contact and $f(\boldsymbol{v})$ is the distribution of velocity assumed to be a Gaussian. These assumptions of molecular chaos and gaussianity of the velocity distribution let us approximate Eq. (C3) to the following form in 2D:

$$\langle A\rangle_{\mathrm{coll}} = \frac{\int_0^\infty \mathrm{d}v \int_{-\pi/2}^{\pi/2}\mathrm{d}\theta\,\cos(\theta)A(v,\theta)\frac{mv^2}{2T}e^{-\frac{1}{2}\frac{mv^2}{2T}}}{2\sqrt{\frac{\pi T}{m}}}. \tag{C5}$$

These assumptions also lead to the Enskog expression for the collision frequency that we used in the main text,

$$\omega(T,\phi g^+) = \langle|\boldsymbol{v}|\rangle/l(\phi) = 8\phi g^+\sqrt{T/(\pi m)}/\sigma. \tag{C6}$$

Equation (C6) can be equivalently obtained from the integration of the loss term in the Boltzmann equation. Indeed, this integral computes the rate at which a particle of *any* velocity changes velocity due to collision, which is by definition the collision frequency.[127]

Equations (C1) and (C5) lead to the following equation for the steady state temperature used in the main text:

$$0 = \frac{\omega}{2}(m\Delta^2 + \alpha\Delta\sqrt{\pi mT} - T(1-\alpha^2)) - 2\gamma(T - T_b). \tag{C7}$$

APPENDIX D: DETAILS CONCERNING THE $\Delta + \gamma$ MODEL

In the $\Delta + \gamma$ model, $T_b = 0$; therefore, $\mathcal{G}$ reduces to

$$\phi g^+ \equiv \mathcal{G}^{\Delta+\gamma} = \frac{\sigma\gamma\sqrt{\pi m}T}{2\sqrt{T}(m\Delta^2 + \alpha\Delta\sqrt{\pi mT} - (1-\alpha^2)T)}, \tag{D1}$$

and $\tilde{p}^{\,\Delta+\gamma}$ reads

$$\tilde{p}^{\,\Delta+\gamma} = T + \mathcal{G}^{\Delta+\gamma}(T)\left((1+\alpha)T + 2\Delta\sqrt{\pi mT}\right). \tag{D2}$$

In order to know whether T_s is larger or smaller than T_l using the inequality $\tilde{p}^{\,\Delta+\gamma}(T_s) < \tilde{p}^{\,\Delta+\gamma}(T_l)$, we must know the variations of $\tilde{p}$. Direct computation of the derivative of $\tilde{p}^{\,\Delta+\gamma}$ with respect to T leads to

$$\frac{\mathrm{d}\tilde{p}^{\,\Delta+\gamma}}{\mathrm{d}T} = 1 + \left(1 + \alpha + \Delta\sqrt{\pi m/T}\right)\mathcal{G}^{\Delta+\gamma} + \left((1+\alpha)T + 2\Delta\sqrt{\pi mT}\right)\frac{\mathrm{d}\mathcal{G}^{\Delta+\gamma}}{\mathrm{d}T}. \tag{D3}$$

Using $m\Delta^2 + \alpha\Delta\sqrt{\pi mT} - (1-\alpha^2)T = 4\gamma T/\omega > 0$ [Eq. (C7)], we can show that $\frac{\mathrm{d}\mathcal{G}^{\Delta+\gamma}}{\mathrm{d}T} > 0$ and $\mathcal{G}^{\Delta+\gamma} > 0$, from which we obtain that $\mathrm{d}\tilde{p}^{\,\Delta+\gamma}/\mathrm{d}T > 0$. This proves that $\tilde{p}^{\,\Delta+\gamma}$ is a continuous and increasing function of the relevant temperatures.

Using the monotonous increase of $\tilde{p}^{\Delta+\gamma}$, we finally arrive at our result,

$$\tilde{p}^{\Delta+\gamma}(T_s^{\Delta+\gamma}) < \tilde{p}^{\Delta+\gamma}(T_l^{\Delta+\gamma}) \Rightarrow T_s^{\Delta+\gamma} < T_l^{\Delta+\gamma}, \tag{D4}$$

which shows that the solid is colder than the liquid at coexistence in the $\Delta + \gamma$ model.

APPENDIX E: DETAILS CONCERNING THE GLM

In the GLM, $\Delta = 0$; therefore, $\mathcal{G}$ simplifies to

$$\phi g^+ \equiv \mathcal{G}^{\mathrm{GLM}} = \frac{\sigma\gamma\sqrt{\pi m}(T_b - T)}{2(1-\alpha^2)T^{3/2}}, \tag{E1}$$

and $\tilde{p}^{\mathrm{GLM}}$ reads

$$\begin{aligned}\tilde{p}^{\mathrm{GLM}} &= T\big(1 + \mathcal{G}^{\mathrm{GLM}}(T)(1+\alpha)\big)\\ &= T_b\tilde{T}\Big(1 + \Lambda(1-\tilde{T})\tilde{T}^{-3/2}\Big),\end{aligned} \tag{E2}$$

with $\tilde{T} = T/T_b$ and $\Lambda = \frac{\gamma\sigma\sqrt{\pi m/T_b}}{2(1-\alpha)} > 0$, a dimensionless parameter such that, when molecular chaos holds and velocities follow a Gaussian distribution, $\Lambda \to \infty$ corresponds to an equilibrium limit.

Since the bath is the only source of energy injection in the system, physical temperatures must respect $T < T_b$ and, hence, $\tilde{T} < 1$. We can, therefore, restrict our attention to the behavior of $\tilde{p}^{\mathrm{GLM}}$ at $\tilde{T} < 1$. In order to know whether T_s is larger or smaller than T_l using the inequality $\tilde{p}^{\mathrm{GLM}}(T_s^{\mathrm{GLM}}) < \tilde{p}^{\mathrm{GLM}}(T_l^{\mathrm{GLM}})$, we must know the variations of $\tilde{p}^{\mathrm{GLM}}$. Direct computation of the derivative of $\tilde{p}^{\mathrm{GLM}}$ with respect to T leads to

$$\frac{\mathrm{d}\tilde{p}^{\mathrm{GLM}}}{\mathrm{d}T} = T_b\left(1 - \frac{\Lambda}{2}(1+\tilde{T})\tilde{T}^{-3/2}\right). \tag{E3}$$

Equation (E3) implies that $\tilde{p}^{\mathrm{GLM}}$ is decreasing from 0 to $\tilde{T}^\star$ and then increasing from $\tilde{T}^\star$ to ∞, where $\tilde{T}^\star$ is the unique real root of Eq. (E3) given by a third order polynomial in $\tilde{T}^{1/2}$,

$$2(\tilde{T}^\star)^{3/2} - \Lambda(1+\tilde{T}^\star) = 0. \tag{E4}$$

We now perform an asymptotic expansion around $\Lambda = 1$ where the solution $\tilde{T}^\star = 1$ of the polynomial Eq. (E4) is known,

$$\begin{aligned}\Lambda &= 1 + \varepsilon,\\ \tilde{T}^\star &= 1 + \sum_{i=1}^{\infty} a_i \varepsilon^i.\end{aligned} \tag{E5}$$

Inserting Eq. (E5) in Eq. (E4) and solving order by order leads to the following approximation for the root of Eq. (E3):

$$\tilde{T}^* = 1 + (\Lambda - 1) + \frac{1}{8}(\Lambda-1)^2 + \mathcal{O}\big((\Lambda-2)^3\big). \tag{E6}$$

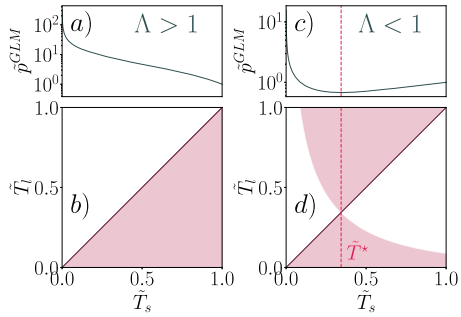

FIG. 4. Typical behavior of $\tilde{p}^{\mathrm{GLM}}$ and $\tilde{p}^{\mathrm{GLM}}(T_s) < \tilde{p}^{\mathrm{GLM}}(T_l)$ for $\Lambda > 1$ and $\Lambda < 1$. (a) and (c) Evolution of $\tilde{p}^{\mathrm{GLM}}$ as a function of $\tilde{T}$. For $\Lambda > 1$, $\tilde{p}$ is purely decreasing, while for $\Lambda > 1$, $\tilde{p}^{\mathrm{GLM}}$ has a change of variation at $\tilde{T}^\star$. (b) and (d) The corresponding regions that verify $\tilde{p}^{\mathrm{GLM}}(T_s) < \tilde{p}^{\mathrm{GLM}}(T_l)$. The shaded regions are the regions in which the inequality holds. For $\Lambda > 1$, we obtain $\tilde{T}_s > \tilde{T}_l$. However, for $\Lambda < 1$, both scenarios are possible. Hence, determining whether $\tilde{T}_s > \tilde{T}_l$ requires estimates for ϕg^+.

For $\Lambda > 1$, as it is clear that the exact root $\tilde{T}^\star(\Lambda)$ is monotonically increasing, it must satisfy $\tilde{T}^\star > 1$; therefore, for the physically accessible temperatures ($\tilde{T} < 1$), $\tilde{p}^{\mathrm{GLM}}$ is decreasing, which implies

$$\begin{aligned}&\tilde{p}^{\mathrm{GLM}}(T_s^{\mathrm{GLM}}) < \tilde{p}^{\mathrm{GLM}}(T_l^{\mathrm{GLM}})\\ &\Downarrow \Lambda > 1\\ &T_s^{\mathrm{GLM}} > T_l^{\mathrm{GLM}}.\end{aligned} \tag{E7}$$

This behavior of $\tilde{p}^{\mathrm{GLM}}$ is exemplified in Fig. 4(a), and the corresponding constraints on $\tilde{T}_s$ and $\tilde{T}_l$ are given by Fig. 4(b), where the shaded area is the region in which the inequality Eq. (17) is verified.

In contrast, when $\Lambda < 1$, $\tilde{p}^{\mathrm{GLM}}$ changes from being decreasing to increasing at a value of $\tilde{T}^*$ between 0 and 1. Hence, the constraint on the pressure alone does not determine which phase is hotter. This is exemplified in Figs. 4(c) and 4(d). However, in this limit, the system was typically always observed to crystallize via a continuous transition, rather than through a phase coexistence, in numerical simulations (see Appendix B).

REFERENCES

[1] J. W. Gibbs, "On the equilibrium of heterogeneous substances," Am. J. Sci. **s3-16**(96), 441–458 (1878).
[2] M. E. Cates and J. Tailleur, "Motility-induced phase separation," Annu. Rev. Condens. Matter Phys. **6**(1), 219–244 (2015).
[3] M. E. Cates and C. Nardini, "Active phase separation: New phenomenology from non-equilibrium physics," arXiv:2412.02854 (2024).
[4] F. Schlögl, "Chemical reaction models for non-equilibrium phase transitions," Z. Phys. **253**(2), 147–161 (1972).
[5] S. Mandal, B. Liebchen, and H. Löwen, "Motility-induced temperature difference in coexisting phases," Phys. Rev. Lett. **123**(22), 228001 (2019).
[6] M. N. van der Linden, L. C. Alexander, D. G. A. L. Aarts, and O. Dauchot, "Interrupted motility induced phase separation in aligning active colloids," Phys. Rev. Lett. **123**(9), 098001 (2019).
[7] M. E. Cates, D. Marenduzzo, I. Pagonabarraga, and J. Tailleur, "Arrested phase separation in reproducing bacteria creates a generic route to pattern formation," Proc. Natl. Acad. Sci. U. S. A. **107**(26), 11715–11720 (2010).

[8]E. Mani and H. Löwen, "Effect of self-propulsion on equilibrium clustering," Phys. Rev. E **92**(3), 032301 (2015).
[9]V. Prymidis, H. Sielcken, and L. Filion, "Self-assembly of active attractive spheres," Soft Matter **11**(21), 4158–4166 (2015).
[10]S. Saha, R. Golestanian, and S. Ramaswamy, "Clusters, asters, and collective oscillations in chemotactic colloids," Phys. Rev. E **89**(6), 062316 (2014).
[11]B. Liebchen, D. Marenduzzo, I. Pagonabarraga, and M. E. Cates, "Clustering and pattern formation in chemorepulsive active colloids," Phys. Rev. Lett. **115**(25), 258301 (2015).
[12]R. Matas-Navarro, R. Golestanian, T. B. Liverpool, and S. M. Fielding, "Hydrodynamic suppression of phase separation in active suspensions," Phys. Rev. E **90**(3), 032304 (2014).
[13]S. Thutupalli, D. Geyer, R. Singh, R. Adhikari, and H. A. Stone, "Flow-induced phase separation of active particles is controlled by boundary conditions," Proc. Natl. Acad. Sci. U. S. A. **115**(21), 5403–5408 (2018).
[14]R. Wittkowski, A. Tiribocchi, J. Stenhammar, R. J. Allen, D. Marenduzzo, and M. E. Cates, "Scalar φ^4 field theory for active-particle phase separation," Nat. Commun. **5**(1), 4351 (2014).
[15]A. P. Solon, J. Stenhammar, M. E. Cates, Y. Kafri, and J. Tailleur, "Generalized thermodynamics of motility-induced phase separation: Phase equilibria, Laplace pressure, and change of ensembles," New J. Phys. **20**(7), 075001 (2018).
[16]A. K. Omar, H. Row, S. A. Mallory, and J. F. Brady, "Mechanical theory of nonequilibrium coexistence and motility-induced phase separation," Proc. Natl. Acad. Sci. U. S. A. **120**(18), e2219900120 (2023).
[17]F. Caballero, A. Maitra, and C. Nardini, "Interface dynamics of wet active systems," Phys. Rev. Lett. **134**(8), 087105 (2025).
[18]M. Besse, G. Fausti, M. E. Cates, B. Delamotte, and C. Nardini, "Interface roughening in nonequilibrium phase-separated systems," Phys. Rev. Lett. **130**(18), 187102 (2023).
[19]X.-q. Shi, G. Fausti, H. Chaté, C. Nardini, and A. Solon, "Self-organized critical coexistence phase in repulsive active particles," Phys. Rev. Lett. **125**(16), 168001 (2020).
[20]S. Pattanayak, S. Mishra, and S. Puri, "Ordering kinetics in the active model B," Phys. Rev. E **104**(1), 014606 (2021).
[21]G. Fausti, M. E. Cates, and C. Nardini, "Statistical properties of microphase and bubbly phase-separated active fluids," Phys. Rev. E **110**(4), L042103 (2024).
[22]E. Tjhung, C. Nardini, and M. E. Cates, "Cluster phases and bubbly phase separation in active fluids: Reversal of the Ostwald process," Phys. Rev. X **8**(3), 031080 (2018).
[23]C. B. Caporusso, P. Digregorio, D. Levis, L. F. Cugliandolo, and G. Gonnella, "Motility-induced microphase and macrophase separation in a two-dimensional active Brownian particle system," Phys. Rev. Lett. **125**(17), 178004 (2020).
[24]A. K. Omar, Z.-G. Wang, and J. F. Brady, "Microscopic origins of the swim pressure and the anomalous surface tension of active matter," Phys. Rev. E **101**(1), 012604 (2020).
[25]L. Langford and A. K. Omar, "The mechanics of nucleation and growth and the surface tensions of active matter," arXiv:2407.06462 (2024).
[26]A. Patch, D. M. Sussman, D. Yllanes, and M. C. Marchetti, "Curvature-dependent tension and tangential flows at the interface of motility-induced phases," Soft Matter **14**(36), 7435–7445 (2018).
[27]R. Zakine, Y. Zhao, M. Knežević, A. Daerr, Y. Kafri, J. Tailleur, and F. van Wijland, "Surface tensions between active fluids and solid interfaces: Bare vs dressed," Phys. Rev. Lett. **124**(24), 248003 (2020).
[28]S.-i. Sasa and N. Nakagawa, "Non-equilibrium phase coexistence in boundary-driven diffusive systems," J. Stat. Phys. **192**(2), 26 (2025).
[29]N. Nakagawa and S.-i. Sasa, "Liquid-gas transitions in steady heat conduction," Phys. Rev. Lett. **119**(26), 260602 (2017).
[30]A. Yoshida, N. Nakagawa, and S.-i. Sasa, "Heat-induced liquid hovering in liquid-gas coexistence under gravity," Phys. Rev. Lett. **133**(11), 117101 (2024).
[31]M. Kobayashi, N. Nakagawa, and S.-i. Sasa, "Control of metastable states by heat flux in the Hamiltonian potts model," Phys. Rev. Lett. **130**(24), 247102 (2023).
[32]S.-i. Sasa, N. Nakagawa, M. Itami, and Y. Nakayama, "Stochastic order parameter dynamics for phase coexistence in heat conduction," Phys. Rev. E **103**(6), 062129 (2021).
[33]V. Ouazan-Reboul, J. Agudo-Canalejo, and R. Golestanian, "Self-organization of primitive metabolic cycles due to non-reciprocal interactions," Nat. Commun. **14**(1), 4496 (2023).
[34]M. Fruchart, R. Hanai, P. B. Littlewood, and V. Vitelli, "Non-reciprocal phase transitions," Nature **592**(7854), 363–369 (2021).
[35]L. Butzhammer, S. Völkel, I. Rehberg, and K. Huang, "Pattern formation in wet granular matter under vertical vibrations," Phys. Rev. E **92**(1), 012202 (2015).
[36]I. H. Ansari, N. Rivas, and M. Alam, "Phase-coexisting patterns, horizontal segregation, and controlled convection in vertically vibrated binary granular mixtures," Phys. Rev. E **97**(1), 012911 (2018).
[37]Y.-J. Chiu and A. K. Omar, "Phase coexistence implications of violating Newton's third law," J. Chem. Phys. **158**(16), 164903 (2023).
[38]H. Löwen, "Inertial effects of self-propelled particles: From active Brownian to active Langevin motion," J. Chem. Phys. **152**(4), 040901 (2020).
[39]L. Caprini, U. Marini Bettolo Marconi, and A. Puglisi, "Spontaneous velocity alignment in motility-induced phase separation," Phys. Rev. Lett. **124**(7), 078001 (2020).
[40]L. Caprini and U. Marini Bettolo Marconi, "Inertial self-propelled particles," J. Chem. Phys. **154**(2), 024902 (2021).
[41]L. Caprini, R. K. Gupta, and H. Löwen, "Role of rotational inertia for collective phenomena in active matter," Phys. Chem. Chem. Phys. **24**(40), 24910–24916 (2022).
[42]Y. Kuroda, H. Matsuyama, T. Kawasaki, and K. Miyazaki, "Anomalous fluctuations in homogeneous fluid phase of active Brownian particles," Phys. Rev. Res. **5**(1), 013077 (2023).
[43]A. Suma, G. Gonnella, D. Marenduzzo, and E. Orlandini, "Motility-induced phase separation in an active dumbbell fluid," Europhys. Lett. **108**(5), 56004 (2014).
[44]L. Hecht, S. Mandal, H. Löwen, and B. Liebchen, "Active refrigerators powered by inertia," Phys. Rev. Lett. **129**(17), 178001 (2022).
[45]L. Hecht, L. Caprini, H. Löwen, and B. Liebchen, "How to define temperature in active systems?," J. Chem. Phys. **161**(22), 224904 (2024).
[46]L. Caprini, D. Breoni, A. Ldov, C. Scholz, and H. Löwen, "Dynamical clustering and wetting phenomena in inertial active matter," Commun. Phys. **7**(1), 343 (2024).
[47]L. Hecht, I. Dong, and B. Liebchen, "Motility-induced coexistence of a hot liquid and a cold gas," Nat. Commun. **15**(1), 3206 (2024).
[48]D. Risso, R. Soto, and M. Guzmán, "Effective two-dimensional model for granular matter with phase separation," Phys. Rev. E **98**(2), 022901 (2018).
[49]J. P. D. Clewett, J. Wade, R. M. Bowley, S. Herminghaus, M. R. Swift, and M. G. Mazza, "The minimization of mechanical work in vibrated granular matter," Sci. Rep. **6**(1), 28726 (2016).
[50]C. Cartes, M. G. Clerc, and R. Soto, "van der Waals normal form for a one-dimensional hydrodynamic model," Phys. Rev. E **70**(3), 031302 (2004).
[51]E. Khain and I. S. Aranson, "Hydrodynamics of a vibrated granular monolayer," Phys. Rev. E **84**(3), 031308 (2011).
[52]M. Argentina, M. G. Clerc, and R. Soto, "van der Waals–like transition in fluidized granular matter," Phys. Rev. Lett. **89**(4), 044301 (2002).
[53]S. Herminghaus and M. G. Mazza, "Phase separation in driven granular gases: Exploring the elusive character of nonequilibrium steady states," Soft Matter **13**(5), 898–910 (2017).
[54]E. Khain, B. Meerson, and P. V. Sasorov, "Phase diagram of van der Waals–like phase separation in a driven granular gas," Phys. Rev. E **70**(5), 051310 (2004).
[55]E. Khain and B. Meerson, "Oscillatory instability in a driven granular gas," Europhys. Lett. **65**(2), 193 (2004).
[56]J. J. Brey, V. Buzón, M. I. García de Soria, and P. Maynar, "Stability analysis of the homogeneous hydrodynamics of a model for a confined granular gas," Phys. Rev. E **93**(6), 062907 (2016).
[57]K. Roeller, J. P. D. Clewett, R. M. Bowley, S. Herminghaus, and M. R. Swift, "Liquid-gas phase separation in confined vibrated dry granular matter," Phys. Rev. Lett. **107**(4), 048002 (2011).
[58]M. Noirhomme, A. Cazaubiel, E. Falcon, D. Fischer, Y. Garrabos, C. Lecoutre-Chabot, S. Mawet, E. Opsomer, F. Palencia, S. Pillitteri, and N. Vandewalle, "Particle dynamics at the onset of the granular gas-liquid transition," Phys. Rev. Lett. **126**(12), 128002 (2021).

[59]M. Noirhomme, A. Cazaubiel, A. Darras, E. Falcon, D. Fischer, Y. Garrabos, C. Lecoutre-Chabot, S. Merminod, E. Opsomer, F. Palencia *et al.*, "Threshold of gas-like to clustering transition in driven granular media in low-gravity environment," Europhys. Lett. **123**(1), 14003 (2018).
[60]Y. Komatsu and H. Tanaka, "Roles of energy dissipation in a liquid-solid transition of out-of-equilibrium systems," Phys. Rev. X **5**(3), 031025 (2015).
[61]M. G. Clerc, P. Cordero, J. Dunstan, K. Huff, N. Mujica, D. Risso, and G. Varas, "Liquid–solid-like transition in quasi-one-dimensional driven granular media," Nat. Phys. **4**(3), 249–254 (2008).
[62]L.-H. Luu, G. Castillo, N. Mujica, and R. Soto, "Capillarylike fluctuations of a solid-liquid interface in a noncohesive granular system," Phys. Rev. E **87**(4), 040202 (2013).
[63]A. Prevost, P. Melby, D. A. Egolf, and J. S. Urbach, "Nonequilibrium two-phase coexistence in a confined granular layer," Phys. Rev. E **70**(5), 050301 (2004).
[64]N. Rivas, P. Cordero, D. Risso, and R. Soto, "Characterization of the energy bursts in vibrated shallow granular systems," Granular Matter **14**, 157–162 (2012).
[65]A. Götzendorfer, J. Kreft, C. A. Kruelle, and I. Rehberg, "Sublimation of a vibrated granular monolayer: Coexistence of gas and solid," Phys. Rev. Lett. **95**(13), 135704 (2005).
[66]P. Melby, F. V. Reyes, A. Prevost, R. Robertson, P. Kumar, D. A. Egolf, and J. S. Urbach, "The dynamics of thin vibrated granular layers," J. Phys.: Condens. Matter **17**(24), S2689 (2005).
[67]J. S. Olafsen and J. S. Urbach, "Clustering, order, and collapse in a driven granular monolayer," Phys. Rev. Lett. **81**, 4369–4372 (1998).
[68]R. Zuñiga, G. Varas, and S. Job, "Geometry-controlled phase transition in vibrated granular media," Sci. Rep. **12**(1), 14989 (2022).
[69]F. V. Reyes and J. S. Urbach, "Effect of inelasticity on the phase transitions of a thin vibrated granular layer," Phys. Rev. E **78**(5), 051301 (2008).
[70]A. E. Lobkovsky, F. V. Reyes, and J. S. Urbach, "The effects of forcing and dissipation on phase transitions in thin granular layers," Eur. Phys. J.: Spec. Top. **179**(1), 113–122 (2009).
[71]G. Gao, Y. Chen, J. Xu, K. Li, and B. Lu, "Temperature inversion across coexisting phases in two-dimensional driven granular materials," Phys. Fluids **36**(12), 123339 (2024).
[72]A. Plati, R. Maire, F. Boulogne, F. Restagno, F. Smallenburg, and G. Foffi, "Self-assembly and non-equilibrium phase coexistence in a binary granular mixture," arXiv:2410.21576 (2024).
[73]R. Maire, A. Plati, M. Stockinger, E. Trizac, F. Smallenburg, and G. Foffi, "Interplay between an absorbing phase transition and synchronization in a driven granular system," Phys. Rev. Lett. **132**(23), 238202 (2024).
[74]A. Plati, R. Maire, E. Fayen, F. Boulogne, F. Restagno, F. Smallenburg, and G. Foffi, "Quasi-crystalline order in vibrating granular matter," Nat. Phys. **20**(3), 465–471 (2024).
[75]G. Castillo, N. Mujica, and R. Soto, "Fluctuations and criticality of a granular solid-liquid-like phase transition," Phys. Rev. Lett. **109**(9), 095701 (2012).
[76]G. Castillo, N. Mujica, and R. Soto, "Universality and criticality of a second-order granular solid-liquid-like phase transition," Phys. Rev. E **91**(1), 012141 (2015).
[77]M. Guzmán and R. Soto, "Critical phenomena in quasi-two-dimensional vibrated granular systems," Phys. Rev. E **97**(1), 012907 (2018).
[78]W. Losert, D. G. W. Cooper, and J. P. Gollub, "Propagating front in an excited granular layer," Phys. Rev. E **59**, 5855–5861 (1999).
[79]G. Castillo, N. Mujica, N. Sepúlveda, J. C. Sobarzo, M. Guzmán, and R. Soto, "Hyperuniform states generated by a critical friction field," Phys. Rev. E **100**(3), 032902 (2019).
[80]P. M. Reis, R. A. Ingale, and M. D. Shattuck, "Crystallization of a quasi-two-dimensional granular fluid," Phys. Rev. Lett. **96**(25), 258001 (2006).
[81]R. Brito, D. Risso, and R. Soto, "Hydrodynamic modes in a confined granular fluid," Phys. Rev. E **87**(2), 022209 (2013).
[82]A. Sarracino, D. Villamaina, G. Costantini, and A. Puglisi, "Granular Brownian motion," J. Stat. Mech.: Theory Exp. **2010**(04), P04013.
[83]A. Puglisi, *Transport and Fluctuations in Granular Fluids: From Boltzmann Equation to Hydrodynamics, Diffusion and Motor Effects* (Springer, 2014).
[84]R. Maire and A. Plati, "Enhancing (quasi-)long-range order in a two-dimensional driven crystal," J. Chem. Phys. **161**(5), 054902 (2024).
[85]E. P. Bernard and W. Krauth, "Two-step melting in two dimensions: First-order liquid-hexatic transition," Phys. Rev. Lett. **107**(15), 155704 (2011).
[86]L. Bai and D. Breen, "Calculating center of mass in an unbounded 2D environment," J. Graphics Tools **13**(4), 53–60 (2008).
[87]C. Maggi, M. Paoluzzi, A. Crisanti, E. Zaccarelli, and N. Gnan, "Universality class of the motility-induced critical point in large scale off-lattice simulations of active particles," Soft Matter **17**(14), 3807–3812 (2021).
[88]J. T. Siebert, F. Dittrich, F. Schmid, K. Binder, T. Speck, and P. Virnau, "Critical behavior of active Brownian particles," Phys. Rev. E **98**(3), 030601 (2018).
[89]F. Smallenburg, "Efficient event-driven simulations of hard spheres," Eur. Phys. J. E **45**(3), 22 (2022).
[90]A. Baldassarri, A. Barrat, G. D'Anna, V. Loreto, P. Mayor, and A. Puglisi, "What is the temperature of a granular medium?," J. Phys.: Condens. Matter **17**(24), S2405 (2005).
[91]A. Puglisi, A. Sarracino, and A. Vulpiani, "Temperature in and out of equilibrium: A review of concepts, tools and attempts," Phys. Rep. **709–710**, 1–60 (2017).
[92]J. E. Mayer and W. W. Wood, "Interfacial tension effects in finite, periodic, two-dimensional systems," J. Chem. Phys. **42**(12), 4268–4274 (1965).
[93]M. Engel, J. A. Anderson, S. C. Glotzer, M. Isobe, E. P. Bernard, and W. Krauth, "Hard-disk equation of state: First-order liquid-hexatic transition in two dimensions with three simulation methods," Phys. Rev. E **87**(4), 042134 (2013).
[94]B. Li, Y. Nishikawa, P. Höllmer, L. Carillo, A. C. Maggs, and W. Krauth, "Hard-disk pressure computations—A historic perspective," J. Chem. Phys. **157**(23), 234111 (2022).
[95]I. Pagonabarraga, E. Trizac, T. P. C. Van Noije, and M. H. Ernst, "Randomly driven granular fluids: Collisional statistics and short scale structure," Phys. Rev. E **65**(1), 011303 (2001).
[96]V. Garzó, R. Brito, and R. Soto, "Enskog kinetic theory for a model of a confined quasi-two-dimensional granular fluid," Phys. Rev. E **98**(5), 052904 (2018).
[97]B. Néel, I. Rondini, A. Turzillo, N. Mujica, and R. Soto, "Dynamics of a first-order transition to an absorbing state," Phys. Rev. E **89**(4), 042206 (2014).
[98]J.-P. Hansen and I. R. McDonald, *Theory of Simple Liquids: With Applications to Soft Matter* (Academic Press, 2013).
[99]G. Gradenigo, A. Sarracino, D. Villamaina, and A. Puglisi, "Fluctuating hydrodynamics and correlation lengths in a driven granular fluid," J. Stat. Mech.: Theory Exp. **2011**(08), P08017.
[100]A. Barrat and E. Trizac, "Molecular dynamics simulations of vibrated granular gases," Phys. Rev. E **66**(5), 051303 (2002).
[101]T. P. C. Van Noije, M. H. Ernst, E. Trizac, and I. Pagonabarraga, "Randomly driven granular fluids: Large-scale structure," Phys. Rev. E **59**(4), 4326 (1999).
[102]M. de Jager, C. Vega, P. Montero de Hijes, F. Smallenburg, and L. Filion, "Statistical mechanics of crystal nuclei of hard spheres," J. Chem. Phys. **161**, 184501 (2024).
[103]N. V. Brilliantov and T. Pöschel, *Kinetic Theory of Granular Gases* (Oxford University Press, 2004).
[104]T. P. C. Van Noije and M. H. Ernst, "Velocity distributions in homogeneous granular fluids: The free and the heated case," Granular Matter **1**(2), 57–64 (1998).
[105]S. E. Esipov and T. Pöschel, "The granular phase diagram," J. Stat. Phys. **86**, 1385–1395 (1997).
[106]G. W. Baxter and J. S. Olafsen, "Experimental evidence for molecular chaos in granular gases," Phys. Rev. Lett. **99**(2), 028001 (2007).
[107]R. Gómez González, V. Garzó, R. Brito, and R. Soto, "Diffusion of impurities in a moderately dense confined granular gas," Phys. Fluids **36**(12), 123387 (2024).

[108]N. V. Brilliantov and T. Pöschel, "Breakdown of the sonine expansion for the velocity distribution of granular gases," Europhys. Lett. **74**(3), 424 (2006).
[109]J.-C. Géminard and C. Laroche, "Energy of a single bead bouncing on a vibrating plate: Experiments and numerical simulations," Phys. Rev. E **68**(3), 031305 (2003).
[110]E. Fayen, A. Jagannathan, G. Foffi, and F. Smallenburg, "Infinite-pressure phase diagram of binary mixtures of (non)additive hard disks," J. Chem. Phys. **152**(20), 204901 (2020).
[111]E. Fayen, M. Impéror-Clerc, L. Filion, G. Foffi, and F. Smallenburg, "Self-assembly of dodecagonal and octagonal quasicrystals in hard spheres on a plane," Soft Matter **19**(14), 2654–2663 (2023).
[112]E. Fayen, L. Filion, G. Foffi, and F. Smallenburg, "Quasicrystal of binary hard spheres on a plane stabilized by configurational entropy," Phys. Rev. Lett. **132**(4), 048202 (2024).
[113]G. M. Rodríguez-Liñán and M. Heinen, "Granular beads in a vibrating, quasi two-dimensional cell: The true shape of the effective pair potential," J. Comput. Phys. **394**, 232–242 (2019).
[114]R. A. Bordallo-Favela, A. Ramírez-Saíto, C. A. Pacheco-Molina, J. A. Perera-Burgos, Y. Nahmad-Molinari, and G. Pérez, "Effective potentials of dissipative hard spheres in granular matter," Eur. Phys. J. E **28**, 395–400 (2009).
[115]S. Velázquez-Pérez, G. Pérez-Ángel, and Y. Nahmad-Molinari, "Effective potentials in a bidimensional vibrated granular gas," Phys. Rev. E **94**(3), 032903 (2016).
[116]J. M. Kosterlitz and D. J. Thouless, "Ordering, metastability and phase transitions in two-dimensional systems," in *Basic Notions of Condensed Matter Physics* (CRC Press, 2018), pp. 493–515.
[117]B. I. Halperin and D. R. Nelson, "Theory of two-dimensional melting," Phys. Rev. Lett. **41**(2), 121 (1978).
[118]D. R. Nelson and B. I. Halperin, "Dislocation-mediated melting in two dimensions," Phys. Rev. B **19**(5), 2457 (1979).
[119]A. P. Young, "Melting and the vector Coulomb gas in two dimensions," Phys. Rev. B **19**(4), 1855 (1979).
[120]V. L. Berezinskii, "Destruction of long-range order in one-dimensional and two-dimensional systems having a continuous symmetry group I. Classical systems," Sov. Phys. JETP **32**(3), 493–500 (1971).
[121]Ó. Toledano, M. Pancorbo, J. E. Alvarellos, and Ó. Gálvez, "Melting in two-dimensional systems: Characterizing continuous and first-order transitions," Phys. Rev. B **103**(9), 094107 (2021).
[122]S. C. Kapfer and W. Krauth, "Two-dimensional melting: From liquid-hexatic coexistence to continuous transitions," Phys. Rev. Lett. **114**(3), 035702 (2015).
[123]L. Galliano, M. E. Cates, and L. Berthier, "Two-dimensional crystals far from equilibrium," Phys. Rev. Lett. **131**(4), 047101 (2023).
[124]Y. Kuroda, T. Kawasaki, and K. Miyazaki, "Long-range translational order and hyperuniformity in two-dimensional chiral active crystal," Phys. Rev. Res. **7**(1), L012048 (2025).
[125]Y.-E. Keta and S. Henkes, "Long-range order in two-dimensional systems with fluctuating active stresses," arXiv:2410.14840 (2024).
[126]R. Soto and M. Mareschal, "Statistical mechanics of fluidized granular media: Short-range velocity correlations," Phys. Rev. E **63**(4), 041303 (2001).
[127]P. Visco, F. van Wijland, and E. Trizac, "Collisional statistics of the hard-sphere gas," Phys. Rev. E **77**(4), 041117 (2008).

The Journal of Chemical Physics

RESEARCH ARTICLE | AUGUST 01 2024

Enhancing (quasi-)long-range order in a two-dimensional driven crystal

R. Maire ; A. Plati

J. Chem. Phys. 161, 054902 (2024)
https://doi.org/10.1063/5.0217958

The Journal of Chemical Physics ARTICLE pubs.aip.org/aip/jcp

Enhancing (quasi-)long-range order in a two-dimensional driven crystal

Cite as: J. Chem. Phys. 161, 054902 (2024); doi: 10.1063/5.0217958
Submitted: 8 May 2024 • Accepted: 14 July 2024 •
Published Online: 1 August 2024

R. Maire and A. Plati[a)]

AFFILIATIONS

Université Paris-Saclay, CNRS, Laboratoire de Physique des Solides, 91405 Orsay, France

[a)]Author to whom correspondence should be addressed: andrea.plati@universite-paris-saclay.fr

ABSTRACT

It has been recently shown that 2D systems can exhibit crystalline phases with long-range translational order showcasing a striking violation of the Hohenberg–Mermin–Wagner (HMW) theorem, which is valid at equilibrium. This is made possible by athermal driving mechanisms that inject energy into the system without exciting long wavelength modes of the density field, thereby inducing hyperuniformity. However, as thermal fluctuations are superimposed on the non-equilibrium driving, long-range translational order is inevitably lost. Here, we discuss the possibility of exploiting non-equilibrium effects to suppress arbitrarily large density fluctuations even when a global thermal bath is coupled to the system. We introduce a model of a harmonic crystal driven both by a global thermal bath and by a momentum conserving noise, where the typical observables related to density fluctuations and long-range translational order can be analytically derived and put in relation. This model allows us to rationalize the violation of the HMW theorem observed in previous studies through the prediction of large-wavelength phonons, which thermalize at a vanishing effective temperature when the global bath is switched off. The conceptual framework introduced through this theory is then applied to numerical simulations of a hard-disk solid in contact with a thermal bath and driven out-of-equilibrium by active collisions. Our numerical analysis demonstrates how varying driving and dissipative parameters can lead to an arbitrary enhancement of the quasi-long-range order in the system regardless of the applied global noise amplitude. Finally, we outline a possible experimental procedure to apply our results to a realistic granular system.

I. INTRODUCTION

The celebrated Hohenberg–Mermin–Wagner (HMW) theorem[1–3] is a cornerstone of equilibrium statistical mechanics. It establishes the impossibility of obtaining long-range order through continuous symmetry breaking in 1D and 2D equilibrium spin systems with short-range interactions at finite temperature. Similarly, 2D crystals with short-range interactions exhibit a translational quasi-long-range order with a correlation function decaying as a power law due to strong phonon excitations at arbitrarily large length scales.[4] However, their bond-orientational order is long range.[5–8]

While the HMW theorem arises from equilibrium statistical physics, the majority of systems encountered in nature operate out-of-equilibrium. Consequently, the applicability of the theorem to such systems is not assured. As an example, a notable breakdown is observed in the flocking behavior of birds.[9] This process can be modeled by an active XY model, the Vicsek model,[10] showcasing spin–spin long-range order in 2D,[11–15] in clear violation of the HMW theorem. Various studies have further explored potential violations of this theorem in non-equilibrium spin-like systems due to forcing at multiple temperatures;[16,17] advection of the order parameter through a shear flow;[18–22] or a colored noise.[23,24] These ingredients have been shown to be crucial in order to obtain spin–spin long-range order, which, in turn, can be easily destabilized by other out-of-equilibrium effects.[25] However, until recently, the prerequisites for translational long-range order in 2D crystals remained unknown. Indeed, while exceptions were found in nematic crystals[26] or chiral active matter,[27] Mermin–Wagner fluctuations are usually found to be enhanced in the presence of active forces,[28–30] and as a result, an increase in the lower critical dimension is often observed due to giant number fluctuations.[31,32]

However, Galliano *et al.* presented compelling evidence of the breakdown of the HMW theorem in 2D crystalline systems[33] formed

in the active state of a random organization model. The authors showed that, unlike in short-ranged equilibrium systems, a simple non-equilibrium hyperuniform crystal exhibits a translational long-range order, as already hinted in Refs. 34 and 35, due to the absence of thermal fluctuations at a large length scale.

Given these premises, it is important to point out that the recent observations of crystalline phases with long-range translational order in two dimensions only concern models where thermal-like fluctuations are absent by construction.[27,33,36,37] These studies leave open the following key question: how is the translational order affected when thermal fluctuations cannot be neglected?

To tackle this question, in this article, we will investigate the limits of the HMW theorem and its potential breakdown in non-equilibrium systems through a theoretical model of a harmonic crystal coupled to a local bath conserving the center of mass (COM) and a global thermal-like bath. We will show that for this system, the decay of the translational long-range order is controlled by the temperature of the COM and not by the overall kinetic energy, as expected at equilibrium.[4] This theory includes the case of a true long-range translational order as a particular limit and allows quantifying deviations from it due to thermal effects.

Next, we apply our theory to the time-continuous analog[38] of a discrete random organization model in which thermal fluctuations are taken into account. It consists of a hard-disk solid in contact with a thermal bath and driven out-of-equilibrium by active collisions. Through numerical simulations, we show that, in the absence of thermal fluctuations, this system exhibits a hyperuniform long-range ordered 2D crystal in agreement with the phenomenology observed in Refs. 33 and 36. However, when thermal-like motion is taken into account, perfect long-range order is lost. Despite this, we demonstrate how exploiting the non-equilibrium properties of the model enables us to suppress arbitrarily large density fluctuations. This makes it possible to enhance the quasi-long-range translational order in a non-equilibrium crystal without the need to neglect or fine-tune thermal fluctuations. Our model will also serve as a coarse-grained representation of a confined quasi-2D vibrated granular system[38] thus naturally providing a platform for investigating the enhancement of quasi-long-range translational order in experimental systems.

The paper is organized as follows: in Sec. II, we introduce the theoretical model for a harmonic crystal and derive the analytical expression of the typical observables related to density fluctuations and long-range translational order. In Sec. III, we report the numerical results for the non-equilibrium hard-disk solids. Finally, Sec. IV contains the conclusion and a brief discussion about a possible experimental procedure to enhance quasi-long-range order in a realistic granular system.

II. THEORY

A. The model

We study a 2D crystal made of N particles with masses m arranged on a periodic lattice of size $L \times L$ and lattice spacing a. Each particle on the lattice site $\boldsymbol{n}$ interacts with its neighbors $\{\tilde{\boldsymbol{n}}\}$ via a harmonic interaction K. In addition, every particle is coupled to two baths: a global one and a local one, which conserves the momentum and COM. In order to have a well-defined equilibrium limit, both of them separately respect the fluctuation dissipation theorem (FDT).[39–42] From a physical standpoint, the global bath can emerge from the coarse-graining of an external energy source, such as in the case of colloids diffusing in a fluid or beads vibrating on a rough surface, while the local bath is more likely to come from an internal source, such as collisions between particles, as with the noise current in fluctuating hydrodynamics.[43–46] The displacement $\boldsymbol{u}_n$ of each particle at lattice site $\boldsymbol{n}$ with respect to their ideal lattice position is described by the following Langevin equation:

$$m\ddot{\boldsymbol{u}}_n = -K\sum_{\{\tilde{n}\}}(\boldsymbol{u}_n - \boldsymbol{u}_{\tilde{n}}) + \boldsymbol{F}_{com} + \boldsymbol{F}_{loc}. \tag{1}$$

The first term on the right-hand side of the equation represents the harmonic interaction between the nearest neighbors.

The second term $\boldsymbol{F}_{com}$ represents the coupling between the system and a global bath, which does not conserve the position of the COM,

$$\boldsymbol{F}_{com} = -\gamma_{com}\dot{\boldsymbol{u}}_n + \sqrt{2\gamma_{com}T_{com}}\boldsymbol{\xi}_n, \tag{2}$$

where γ_{com} is a global damping and T_{com} is the temperature of the bath. The spatial components α of the white noise are Gaussian and uncorrelated, with zero average,

$$\langle \xi_n^\alpha(t)\xi_m^\beta(t')\rangle = \delta(t-t')\delta_{n,m}\delta^{\alpha,\beta} \qquad \langle \boldsymbol{\xi}_n(t)\rangle = 0. \tag{3}$$

Finally, the last term in Eq. (1) represents a second bath, at temperature T_{loc}, conserving the momentum and the position of the COM. To fulfill this requirement, we use a discretized version of Model B,[47–53]

$$\boldsymbol{F}_{loc} = -\gamma_{loc}\sum_{\{\tilde{n}\}}(\dot{\boldsymbol{u}}_n - \dot{\boldsymbol{u}}_{\tilde{n}}) + \sqrt{2\gamma_{loc}T_{loc}}(\nabla\cdot\boldsymbol{\Xi}_n). \tag{4}$$

The conservation of $\sum_n \dot{\boldsymbol{u}}_n$ is ensured by a discrete Laplacian of $\dot{\boldsymbol{u}}$ for the damping γ_{loc}, taken to be the average over first neighbors and a discrete divergence acting on a rank 2 random tensor $\boldsymbol{\Xi}$. This type of damping naturally arises in granular gases where collisions tend to align particles,[54] in active matter with effective alignment[46,55] or in dissipative particle dynamics.[56–58] More generally, with the corresponding equilibrium noise, it plays the role of a discrete hydrodynamic viscosity and can be derived from the Mori–Zwanzig formalism.[59] It should be noted that if every particle moves in the same direction, then neither damping nor noise is applied, in line with the idea that this local noise might arise from collisions between particles and acts locally. Our model constitutes a simplified lattice equivalent to a fluctuating hydrodynamics description of a solid.[60–66] The variance and the average of the rank 2 tensor $\boldsymbol{\Xi}_n$ are fully determined by our assumption that the FDT holds separately for both noises,[42,67]

$$\langle \Xi_n^{\alpha,\mu}(t)\Xi_m^{\beta,\nu}(t')\rangle = \delta(t'-t)\delta^{\alpha,\beta}\delta^{\mu,\nu}\delta_{n,m}. \tag{5}$$

We further discuss the peculiarity of the noise as well as the expression of the discrete Laplacian and divergence in Appendix A following Ref. 68.

For simplicity, in the following, we chose to work in the Fourier space by performing a semi-discrete Fourier transform (see Appendix B) on Eq. (1),[69,70]

$$\left(-mw^2 - iw(\gamma_{com} + \gamma_{loc}\omega_k^2) + K\omega_k^2\right)\tilde{\boldsymbol{u}}_k = \sqrt{2\gamma_{com}T_{com}}\tilde{\boldsymbol{\xi}}_k + \sqrt{2\gamma_{loc}\omega_k^2 T_{loc}}\tilde{\boldsymbol{\eta}}_k, \quad (6)$$

with ω_k being the dispersion relation of the lattice divided by the natural frequency of the lattice $\sqrt{K/m}$ or equivalently, the eigenvalue of the discrete Laplacian. For instance, in a square lattice, $\omega_k^2 = 2(2 - \cos(k_x a) - \cos(k_y a))$. Both noises have unit variance and zero average, and from a Fourier transform, we obtain

$$\begin{aligned} \langle \tilde{\xi}_k^\alpha(w)\tilde{\xi}_q^\beta(w')\rangle &= \delta(w+w')\delta_{q,-k}\delta^{\alpha,\beta} \qquad \langle \tilde{\xi}_k^\alpha(w)\rangle = 0, \\ \langle \tilde{\eta}_k^\alpha(w)\tilde{\eta}_q^\beta(w')\rangle &= \delta(w+w')\delta_{q,-k}\delta^{\alpha,\beta} \qquad \langle \tilde{\eta}_k^\alpha(w)\rangle = 0. \end{aligned} \quad (7)$$

The noises are simple to generate in the reciprocal space compared to the ones in real space. Moreover, we clearly see that the local bath does not act on the COM since it vanishes at $\boldsymbol{k} = 0$, implying that, as wanted, the motion of the COM is completely governed by the global bath.

Due to the harmonicity of the crystal, Eq. (6) is non-interacting in the k space and every mode reaches an independent equilibrium-like steady state at an effective k-dependent temperature,

$$\tilde{T}_k = \frac{\gamma_{com}T_{com} + \gamma_{loc}\omega_k^2 T_{loc}}{\gamma_{com} + \gamma_{loc}\omega_k^2}. \quad (8)$$

Since the dispersion relation vanishes at low k: $\omega_k^2 \sim (a\boldsymbol{k})^2$,[70] we obtain the two limiting cases,

$$\begin{aligned} \tilde{T}_{k\to 0} &= T_{com}, \\ \tilde{T}_{k\to\infty} &= T_{loc} \quad \text{if} \quad \gamma_{loc} \gg \gamma_{com}. \end{aligned} \quad (9)$$

That is, the large length scale temperature is controlled by T_{com} since the energy created on small length scales by the local bath is damped by γ_{com} on every scale. While the small length scale temperature is controlled by both the global and local bath, in the following, we will assume that the system is more weakly coupled to the local bath compared to the global bath: $\gamma_{loc} \gg \gamma_{com}$, which leads to $\tilde{T}_{k\to\infty} = T_{loc}$.

The equilibrium-like nature of our equation stems from the assumption that both baths are delta correlated and that each mode is independent to the others in k space. This would not be the case in a realistic system with anharmonic terms, for instance, and could potentially disrupt the picture given in this section. We discuss the case of an anharmonic lattice in Appendix C and argue that the phenomenology described here should not change qualitatively.

B. Hyperuniformity

As already noted in Ref. 33, a key requirement to obtain a long-range ordered 2D crystal is hyperuniformity, i.e., the suppression of density fluctuations at arbitrarily large length scales. Within the context of the proposed theoretical model, we derive here the analytical expression of the structure factor $S(\boldsymbol{k})$ whose vanishing low-$\boldsymbol{k}$ limit indicates the presence of hyperuniformity in a system.[34]

We start by computing the static displacement function (SDF) $C_{uu}(\boldsymbol{k}) \equiv C_{uu}(\boldsymbol{k}, t = 0)$,

$$\begin{aligned} C_{uu}(\boldsymbol{k}) &= \frac{1}{2\pi}\int \mathrm{d}w \langle \tilde{\boldsymbol{u}}_k(w)\cdot\tilde{\boldsymbol{u}}_{-k}(-w)\rangle \\ &= \frac{2}{K}\frac{\gamma_{com}T_{com} + \gamma_{loc}\omega_k^2 T_{loc}}{\omega_k^2(\gamma_{com} + \gamma_{loc}\omega_k^2)} = \frac{2}{K\omega_k^2}\tilde{T}_k, \end{aligned} \quad (10)$$

where Eqs. (6) and (7) have been used to calculate averages over the noise. The above-mentioned identity represents the equipartition of elastic energy at an effective temperature $\tilde{T}_k$, which is given by Eq. (8). The standard equipartition theorem for phonons $K\omega_k^2 C_{uu}(\boldsymbol{k})/2 = T_{loc}$ or $K\omega_k^2 C_{uu}(\boldsymbol{k})/2 = T_{com}$ is recovered in the three equilibrium limits of the model, that is, either when $\gamma_{com} = 0, \gamma_{loc} = 0$ or $T_{com} = T_{loc}$. In the large lengths limit, where $\omega_k^2 \sim (a\boldsymbol{k})^2$, the SDF reads

$$C_{uu}(\boldsymbol{k}) = \frac{2T_{com}}{K(a\boldsymbol{k})^2} + \frac{2\gamma_{loc}(T_{loc} - T_{com})}{K\gamma_{com}} + \mathcal{O}\left((T_{loc} - T_{com})(a\boldsymbol{k})^2\right) \quad (11)$$

and diverges as $1/(a\boldsymbol{k})^2$ at equilibrium or more generally when $T_{com} \neq 0$. However, when $T_{com} = 0$ and $\gamma_{com} \neq 0$, the phonons created locally are damped over large distances, and long wavelength phonons are completely suppressed since their elastic energy $K\omega_k^2 C_{uu}(\boldsymbol{k})/2$ goes to 0. The same type of result can be found for the static velocity factor $mC_{\dot{u}\dot{u}}(\boldsymbol{k})/2 = \tilde{T}_k$ showing a depletion of kinetic energy on large scales.

At this point, it is illuminating to note that the long-range structure factor $S(\boldsymbol{k})$ and the SDF are linked by the relation,:[34,35]

$$\begin{aligned} S(\boldsymbol{k}) &= \left\langle \frac{1}{N}\left|\sum_{\boldsymbol{n}} e^{i\boldsymbol{k}\cdot(a\boldsymbol{n}+\boldsymbol{u}_n)}\right|^2 \right\rangle \\ &= \left\langle |\boldsymbol{k}\cdot\tilde{\boldsymbol{u}}_k|^2\right\rangle + \mathcal{O}\left(|\boldsymbol{k}\cdot\tilde{\boldsymbol{u}}_k|^4\right) \\ &= |\boldsymbol{k}|^2 C_{uu}(|\boldsymbol{k}|) + \mathcal{O}\left(|\boldsymbol{k}\cdot\tilde{\boldsymbol{u}}_k|^4\right), \end{aligned} \quad (12)$$

where we used the fact that in our model the longitudinal dispersion relation is equal to the transversal ones. Otherwise, the last relation only holds for longitudinal polarization of the displacement.[35] In an equilibrium system, the value of the structure factor at $\boldsymbol{k} = 0$ is a constant proportional to the isothermal compressibility and the temperature.[71,72] However in our case, from Eq. (11), it follows that

$$S(\boldsymbol{k}) = \frac{2T_{com}}{Ka^2} + \frac{2\gamma_{loc}(T_{loc} - T_{com})}{\gamma_{com}}\boldsymbol{k}^2 + \mathcal{O}\left((T_{loc} - T_{com})a^2\boldsymbol{k}^4\right). \quad (13)$$

When $T_{com} = 0$ and $\gamma_{com} \neq 0$, since the SDF is finite at low k, the structure factor behaves as $S(\boldsymbol{k}) \sim \boldsymbol{k}^2$, unveiling the hyperuniformity of our non-equilibrium system when the COM position or equivalently the momentum is conserved by the local noise at finite global damping. This aligns with results found in Refs. 33, 50, and 73–77 and confirms that our model includes a suitable limit to study the emergence of long-range order in a dimension lower than three.

C. (Quasi-)long-range order

To quantitatively describe the emergence of long-range order in our model, we consider the crystalline translational correlation function, defined as[78,79]

$$g_G(|\boldsymbol{n}-\boldsymbol{m}|) = \left\langle e^{i\boldsymbol{G}\cdot(\boldsymbol{u}_n-\boldsymbol{u}_m)} \right\rangle = e^{-\langle(\boldsymbol{G}\cdot(\boldsymbol{u}_n-\boldsymbol{u}_m))^2\rangle/2}, \tag{14}$$

where $\boldsymbol{G}$ is one of the inner Bragg-peak vectors of the crystal and the last equality follows from the Gaussianity of the stationary probability distribution function. In a long-range ordered crystal, the correlation function decays to a constant value, while in a quasi-long-range 2D equilibrium crystal, it exhibits an algebraic decay.[4,7,79–82] From Eq. (14), it is clear that the asymptotic behavior of the displacement correlation function $\langle(\boldsymbol{u}_n-\boldsymbol{u}_m)^2\rangle$ governs the translational long-range behavior of the system. Specifically, if the displacement correlation function reaches a constant or decays at large distances, true long-range order is expected; otherwise, only quasi-long-range order or short-range order is found. In the infinite system size limit and at large distances compared to the lattice spacing, it can be approximated as (see Appendix D)

$$\begin{aligned}\langle(\boldsymbol{u}_n-\boldsymbol{u}_m)^2\rangle &\simeq \frac{a^2}{\pi}\int_{\frac{1}{a|\boldsymbol{n}-\boldsymbol{m}|}}^{\frac{\pi}{a}} \mathrm{d}k k C_{uu}(|\boldsymbol{k}|)\\ &\simeq \begin{cases} \dfrac{2T_{com}}{\pi K}\log(\pi|\boldsymbol{n}-\boldsymbol{m}|) & |\boldsymbol{n}-\boldsymbol{m}| \gg \delta^{-1} \\ \dfrac{2T_{loc}}{\pi K}\log(\pi|\boldsymbol{n}-\boldsymbol{m}|)) & |\boldsymbol{n}-\boldsymbol{m}| \ll \delta^{-1}, \end{cases}\end{aligned} \tag{15}$$

where $\omega_k^2 = (a\boldsymbol{k})^2$ was assumed and $\delta = \sqrt{\gamma_{com}/\gamma_{loc}}$ is the adimensionalized natural inverse length scale of the system. At $T_{com} = T_{loc}$, we recover the equilibrium logarithmic increase with distance, proportional to the temperature.[4] In a non-equilibrium setting with $T_{com} \neq T_{loc}$, the divergence is still present, but with T_{com} as the prefactor at large scales and T_{loc} at small scales (still larger than the lattice spacing). The numerical "exact" computation of the integral for a hexagonal lattice and its comparison with our approximate formula are shown in Fig. 1. As expected, the approximations work well at large distances. At short distances, although the global scaling remains the same, strong oscillations appear on top of the logarithmic scaling since the phonons start to feel the discreteness of the lattice. For large δ, the transition between the two regimes happens far away from the lattice spacing, allowing for a large range of values over which both scalings are clear and oscillations small. From Eqs. (14) and (15), we obtain that the translational correlation function exhibits a double power law behavior,

$$g_G(|\boldsymbol{n}-\boldsymbol{m}|) \sim \begin{cases} |\boldsymbol{n}-\boldsymbol{m}|^{-|\boldsymbol{G}|^2 T_{com}/(2\pi K)} & |\boldsymbol{n}-\boldsymbol{m}| \gg \delta^{-1}, \\ |\boldsymbol{n}-\boldsymbol{m}|^{-|\boldsymbol{G}|^2 T_{loc}/(2\pi K)} & |\boldsymbol{n}-\boldsymbol{m}| \ll \delta^{-1}, \end{cases} \tag{16}$$

where the angle average of the dot product appearing in Eq. (14) was taken into account by assuming an isotropic crystal. At non zero T_{com}, the large-scale decay of the correlation function is algebraic, indicating a quasi-long-range order.[83] Nonetheless, in contrast to the equilibrium picture, the average kinetic energy of the system can be arbitrarily high; the only crucial factor for the translational quasi-long-range behavior of the system at large scale is the temperature of the COM or equivalently the temperature of the phonons existing on these scales. We also note that, as expected, when the COM is conserved at finite global damping ($T_{com} = 0$ and $\gamma_{com} \neq 0$), the system displays a genuine long-range order, as observed in Ref. 33, and the HMW theorem is broken.

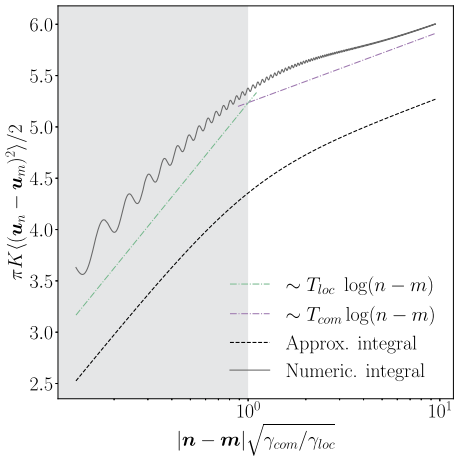

FIG. 1. Numerical and approximate values of $\langle(\boldsymbol{u}_n-\boldsymbol{u}_m)^2\rangle$ at $\gamma_{com}/\gamma_{loc} = 10^{-3}$ given by Eqs. (15) and (D2). For the numerically solved integral, we use the dispersion relation of a hexagonal lattice.

We finally point out that the connection between hyperuniformity and the emergence of a long-range order is made explicit by Eqs. (15) and (12), which show the relationship between the large distance behavior of the displacement correlation function and the low-k limit of the structure factor. Indeed, for large distances, we find in 2D,

$$\begin{aligned}\langle(\boldsymbol{u}_n-\boldsymbol{u}_0)^2\rangle &\propto \int_{\frac{1}{a|\boldsymbol{n}|}}^{\frac{\pi}{a}} \mathrm{d}k\, k C_{uu}(|\boldsymbol{k}|)\\ &\propto \int_{\frac{1}{a|\boldsymbol{n}|}}^{\frac{\pi}{a}} \mathrm{d}k\, \frac{S(|\boldsymbol{k}|)}{k}\\ &\propto \begin{cases} S_0\ \log(|\boldsymbol{n}|) & \text{if } S(k) = S_0 + \mathcal{O}(k), \\ S_1 & \text{if } S(k) = S_1 k^\beta + \mathcal{O}(k^{\beta+1}), \end{cases}\end{aligned} \tag{17}$$

with $\beta > 0$. Moreover, the relation between the structure factor and long-range order is not limited to the particular mechanism of hyperuniformity that we present in this work but is general and also applies for different hyperuniform systems, such as the critical point of absorbing phase transitions.[75]

D. Breakdown of the HMW theorem

The breakdown of the HMW theorem when $T_{com} = 0$ ultimately stems from the fact that large wavelength phonons are thermalized with a bath at 0 effective temperature; a temperature for which, even at equilibrium, long-range order is expected by the HMW theorem. In this sense, the theorem is broken in a way expected from its equilibrium definition while simultaneously being strongly broken since the large-scale SDF at $\boldsymbol{k} \to 0$ is constant and does not diverge at all. This can be traced back to the strong hyperuniformity $S(\boldsymbol{k}) \sim \boldsymbol{k}^2$ of our system. We remark that our rationalization of the emergence of a stable long-range order based on

large wavelength phonons thermalizing at a vanishing effective temperature can also be applied for the non-equilibrium crystal obtained with the random organization model.[33]

It is important to note that an exponent 2 for the small k structure factor is not a necessary condition to break the HMW theorem. Indeed, as understood from Eq. (17), any hyperuniformity in 2D would sufficiently reduce the divergence of the SDF to allow a long-range order. This mechanism parallels bird-flocking dynamics, where alignment among neighbors reduces the infrared divergence of the correlation functions to a scaling of $1/k^a$ with $a < 2$,[11,13] allowing for a long-range order.

From a mathematical point of view, this breakdown of the HMW theorem, in the case $T_{com} = 0$ at finite γ_{com}, is manifested through the regularization of the infrared divergence of the integral used to compute the displacement correlation function [Eq. (D1)] via γ_{com},

$$\langle (\boldsymbol{u}_n - \boldsymbol{u}_m)^2 \rangle \simeq \frac{2a^2}{K\pi} \int_{\frac{1}{a|\boldsymbol{n}-\boldsymbol{m}|}}^{\frac{\pi}{a}} \mathrm{d}k k \left(\frac{1}{\omega_k^2} \frac{T_{com}}{1 + (\omega_k/\delta)^2} + \frac{T_{loc}}{\delta^2 + \omega_k^2} \right). \quad (18)$$

When $T_{com} = 0$, the first term vanishes. In the second term, the phonons exhibit a behavior akin to particles with an effective "mass" $\sqrt{K}\delta = \sqrt{K\gamma_{com}/\gamma_{loc}}$ and an adimensionalized dispersion relation $\Omega_k = \sqrt{\delta^2 + \omega_k^2}$. Indeed, an equilibrium system with Hamiltonian,[70]

$$\mathcal{H}/K = \frac{a^2}{2} \left(2\,\mathrm{Tr}\left[\mathbf{u} \cdot \mathbf{u}^T\right] - \mathrm{Tr}\left[\mathbf{u}\right]^2 \right) + \frac{\delta^2}{2} \boldsymbol{u}^2, \quad (19)$$

with $\mathbf{u}$ being the infinitesimal strain tensor: $\cup = (\nabla \boldsymbol{u} + (\nabla \boldsymbol{u})^T)2$ would produce a similar equilibrium displacement correlation. This effective mass pins down the particles on their ideal lattice position allowing a long-range order. Of course, when $T_{com} \neq 0$, the first term of Eq. (18) becomes significant at small k and induces the logarithmic divergence at large scales discussed above.

It is interesting to note that hyperuniformity of equilibrium crystals is solely achieved through long-range or external interactions,[34] in contrast with our system and that of others, where hyperuniformity is allowed through the breakdown of the FDT and correlated noise.[24,73,84–86] This is reminiscent of long-range correlations induced by a bulk conservation law and dissipation in self-organized criticality.[44,54,87–94] See Ref. 95 for a recent review. Moreover, COM conservation is not the only route to hyperuniformity, and systems with multiplicative[84,96] or time correlated noise can have suppressed long-range fluctuations.[24,36] In addition, recent works on particular non-equilibrium collective excitations in active solids, known as entropons,[69,97] highlight that on a general basis, active forces only add an additional term to the SDF, linked to entropy production but do not affect its phononic part. Thus, active forces alone cannot tame the $1/k^2$ divergence of the phononic part of the equilibrium SDF and, in general, increase the density fluctuations.[28–30] Indeed, active short-ranged systems exhibiting hyperuniformity usually lose this property in the presence of a global thermal equilibrium-like noise.[27,37,98,99] This supports the idea that non-equilibrium-like colored or multiplicative noises are crucial for hyperuniformity and translational long-range order in 2D crystals featuring short-ranged interactions. Further discussions about entropons in our system are provided in Appendix E. However, note that hyperuniformity in passive or active scalar field theories has been found even in the presence of a thermal noise for model B type equations.[100–103]

Of course, the analysis performed so far predicts the violation of the HMW theorem only in the singular limit $T_{com} = 0$ and $\gamma_{com} \neq 0$. However, the results obtained in Sec. II C suggest how to approach this physical condition when $T_{com} \neq 0$. Indeed, the key quantity that controls the strength of the quasi-long-range order (and its possible limit to true long-range) is the exponent of the algebraic decay of the translational correlation function for $|\boldsymbol{n} - \boldsymbol{m}| \gg \delta^{-1}$ in Eq. (16), which is proportional to the ratio T_{com}/K. This means that, for a finite T_{com}, one can still obtain an arbitrary slow decay by increasing the elastic constant K. This is clearly quite a limiting and trivial way to enhance the quasi-long-range order of the system since it consists of a direct increase in the particle interaction strength and would also work at equilibrium. However, in the next section, we will see how the phenomenology of a realistic model of a non-equilibrium crystal can be mapped into one of our model with an effective K, which depends on the non-equilibrium properties of the realistic system (i.e. dissipation and driving parameters). This will be the key point of our strategy to enhance quasi-long-range order through non-equilibrium effects.

III. HARD-DISK CRYSTAL DRIVEN BY ACTIVE COLLISIONS

A. A coarse-grained model

We explore a practical application of our theoretical framework to investigate the breakdown of the HMW theorem and the dependence of (quasi-)long-range order on the noise in realistic non-equilibrium systems. To conduct this investigation, we use the model introduced in Ref. 38 with an additional global noise. This can be thought of as an underdamped continuous-time analog of a random organization model[104] describing sheared suspensions.[105] In the absence of global noise, these models present an absorbing phase transition, are hyperuniform[34] at the transition point[75,84] and, if the COM or momentum is locally conserved by the collisions, in the active state.[73,74,77] As will be further discussed in the conclusion, this model has been used to describe the experimental realization of vibrated quasi-2d granular systems.[38,106,107]

We study this system by performing hybrid event-driven/time-stepped molecular dynamics simulations[108] (see Appendix F) of N active hard disks of diameter σ and mass m in a 2D square of size L with periodic boundary conditions. We define an arbitrary unit of time $\hat{\tau}$. The (granular) temperature T of the system is defined as its global kinetic energy,

$$T = \frac{1}{2} m \sum_{i=1}^{N} \boldsymbol{v}_i^2, \quad (20)$$

with $\boldsymbol{v}_i$ being the velocity of the particle i. The disks experience a global white bath during their free flight,

$$\frac{\mathrm{d}\boldsymbol{v}}{\mathrm{d}t} = -\gamma_{com} \boldsymbol{v} + \sqrt{2\gamma_{com} T_{com}} \boldsymbol{\eta}(t), \quad (21)$$

with

$$\langle \eta_i^\alpha(t) \eta_j^\beta(t') \rangle = \delta(t - t') \delta_{i,j} \delta^{\alpha,\beta}, \qquad \langle \eta_i^\alpha(t) \rangle = 0. \quad (22)$$

Upon collision, two disks undergo a momentum-conserving active collision,[106,109,110]

$$\begin{aligned} \boldsymbol{v}_i' &= \boldsymbol{v}_i + \frac{1+\alpha}{2}(\boldsymbol{v}_{ij}\cdot\hat{\boldsymbol{\sigma}}_{ij})\hat{\boldsymbol{\sigma}}_{ij} + \Delta\hat{\boldsymbol{\sigma}}_{ij}, \\ \boldsymbol{v}_j' &= \boldsymbol{v}_j - \frac{1+\alpha}{2}(\boldsymbol{v}_{ij}\cdot\hat{\boldsymbol{\sigma}}_{ij})\hat{\boldsymbol{\sigma}}_{ij} - \Delta\hat{\boldsymbol{\sigma}}_{ij}, \end{aligned} \tag{23}$$

where $0 \le \alpha \le 1$ is the coefficient of restitution, $\Delta > 0$ is a velocity injection term, $\boldsymbol{v}_i'$ is the post-collision velocity of particle i, $\boldsymbol{v}_i$ is its pre-collision velocity, and $\hat{\boldsymbol{\sigma}}_{ij}$ and $\boldsymbol{v}_{ij}$ are the unit vector joining of particles i and j and the relative velocity between them, respectively. In the limit $\Delta = 0$, the usual collision rule of dissipative hard disks is recovered. This model is similar to the one introduced in Ref. 73 for liquids.

As evidenced by the energy change during a collision,

$$E' - E = m\Delta^2 + m\alpha\Delta|\boldsymbol{v}_{ij}\cdot\hat{\boldsymbol{\sigma}}_{ij}| - m\frac{1-\alpha^2}{4}|\boldsymbol{v}_{ij}\cdot\hat{\boldsymbol{\sigma}}_{ij}|^2, \tag{24}$$

the parameter Δ controls the intensity of the energy injection at collision. These collisions will thus play the role of the momentum-conserving bath introduced in Sec. II at temperature T_{loc} and associated effective damping $\gamma_{loc}\omega_k^2$.

Hence, to recapitulate the differences and similarities between the harmonic crystal presented in the theory and the granular hard disks of interest here, both the models feel an external global Gaussian bath at temperature T_{com} and damping γ_{com}; however, the active collisions in the granular system are modeled as an *effective* local bath at temperature T_{loc} and damping $\gamma_{com}\omega_k^2$ in the theory. From a physical standpoint, the effective T_{loc} in the granular system is technically a function of every parameter of our simulation, including T_{com} and γ_{com}, because the energy change at the collision depends on the relative velocities of the particles colliding, as understood from Eq. (23), which are affected by the global bath and the packing fraction. This will not change the physical picture given in this article; nonetheless, we should keep it in mind. This peculiarity is further discussed in Appendix G.

When $T_{com} = 0$, the collision rule given by Eq. (23) locally conserves the momentum and the position of the COM. Moreover, the global damping in Eq. (21) damps every mode indistinctly. Thus, hyperuniformity is expected,[73] and we recover the system studied in Ref. 38 with an absorbing state at low density (a feature absent in the lattice model because T_{loc} is independent of T_{com} and γ_{com}). Indeed, at low density or packing fraction $\phi = N\pi\sigma^2/4L^2$, the active collisions cannot compensate for the energy dissipated by the drag during the free flight, leading the system to an arrested state. Denser systems attain an active steady state where the energy injection at collision is compensated by the dissipation of the damping.

B. Hyperuniformity and long-range order

To investigate the crystalline order in this system, we simulate crystalline configurations at $\phi = 0.75$, which sets the lattice spacing a. This packing fraction corresponds to systems with long-range bond orientational order at equilibrium[81] but can give rise to a hexatic or a liquid phase in highly dissipative granular systems.[111] To avoid these scenarios, we choose a relatively high $\alpha \ge 0.95$ and always check that the crystalline phase is stable. For simulations at $T_{com} = 0$, we stay away from the absorbing region by choosing γ_{com} and Δ such that ϕ is above the critical packing fraction of the absorbing to active phase transition, and hence, the system has a steady state with finite kinetic energy. Choosing a packing fraction such that $l(\phi) < \Delta/\gamma$ with l the mean free path, ensures a sufficiently high energy injection at collision, which prevents the system from reaching the absorbing state.[38]

We first perform a similar analysis as the one done in Ref. 33, fixing the COM by setting $T_{com} = 0$. The results for three different systems are shown in Fig. 2. Panels (a)–(c) show the structure factor (and the static velocity factor in inset) as a function of k, the long-time behavior of the mean square displacement (MSD) for different system sizes, and finally the translational correlation function as a function of the distance, respectively. The three quantities contain the same information expressed differently. It is illuminating to analyze all three together to better understand the theory given in Sec. II and verify its consistency. We note that the MSD of a particle in a finite crystal reaches a plateau at large times. The value of this plateau is of course dependent not only on the size of the cage made by neighboring particles but also on the collective excitations that induce vibrations on the crystal. From the Fourier transform of the displacement $\tilde{\boldsymbol{u}}_k(w)$, it can be shown that the correlation $\langle(\boldsymbol{u}_n - \boldsymbol{u}_m)^2\rangle$ for an infinite system corresponds to $\mathrm{MSD}(t\to\infty)$ for a system of size $(a|\boldsymbol{m}-\boldsymbol{n}|)^2$ in the large system size limit. We chose to use the MSD instead of the displacement correlation to check relations derived in the theory part involving the displacement correlation, the former being simpler to measure.

We first focus on the curves "*Equilib*," which correspond to an equilibrium system of pure hard disks ($\alpha = 1$, $\Delta = 0$ and $\gamma_{com} = 0$). As expected, its structure factor is approximately flat (it has, in reality, an Ornstein–Zernike shape due to the non-linear interactions[71]) and reaches a well-defined value at small k. Its large time MSD grows as a unique logarithm of the particle number, as predicted by Eq. (15), and thus, its correlation function decreases as a power law with an exponent linked to the logarithmic increase in the MSD, as given by (16) and illustrated with the dashed lines. The system displays a quasi-long-range order.

We now turn to the Δ model, a system with only active collision and no global damping ($\alpha < 1$ and $\Delta \neq 0$ but $\gamma_{com} = 0$). Hence, the dynamics of the system is ballistic between collisions, and the non-equilibrium effects arise purely from the non-equilibrium collision rule Eq. (23). The steady state of this system is the result of an interplay between the energy injected at collision by Δ and dissipated by α, as given by Eq. (24). Under these conditions, the temperature of the system T is a function of α and Δ^2 [see Appendix G, Eq. (G2)], and by definition, it equilibrates to the local bath temperature T_{loc}. Its structure factor has a transient hyperuniform scaling before reaching a plateau at small k. The same behavior is found for the static velocity factor. This is incompatible with the modelization of the active collision as an FDT respecting bath at temperature T_{loc} and damping $\gamma_{loc}\omega_k^2$. Indeed, if the active collisions were acting on a coarse-grained level like such an equilibrium bath, the structure factor should have resembled the *Equilib* one. It can be shown that in a hydrodynamic description,[106] the fast temperature field is highly out-of-equilibrium and acts as a genuinely non-equilibrium bath for the slow velocity field. This effect induces the observed decay. This is, however, not the main concern of this paper and does not change the phenomenology observed when an additional global damping is added. Hence, the study of this peculiar bath is left for future

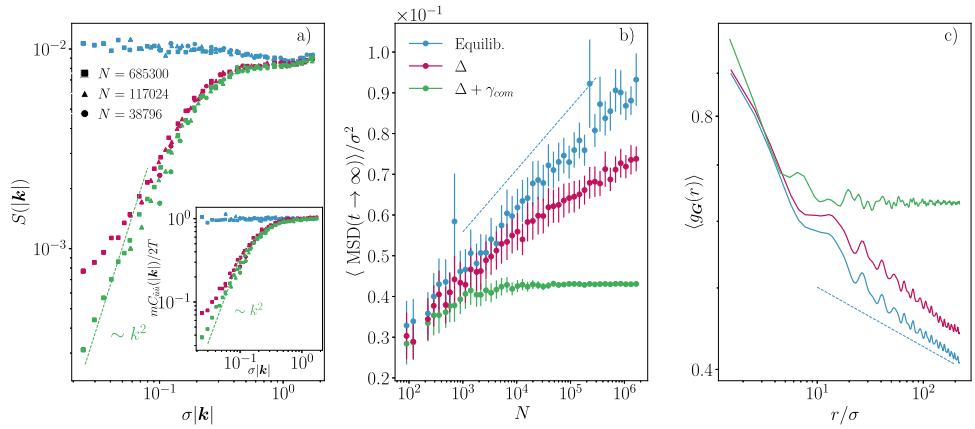

FIG. 2. Long-range behavior of three different crystalline systems with $T_{com} = 0$. "*Equilib.*" corresponds to pure hard disks ($\alpha = 1$, $\Delta/\sigma\hat{\tau}^{-1} = 0$, and $\gamma_{com} = 0$); "Δ" corresponds to hard disks with active collisions ($\alpha = 0.95$, $\Delta/\sigma\hat{\tau}^{-1} = 0.015$, and $\gamma_{com}/\hat{\tau} = 0$); and "$\Delta + \gamma_{com}$" corresponds to hard disks with active collisions and global damping ($\alpha = 0.95$, $\Delta/\sigma\hat{\tau}^{-1} = 0.015$, and $\gamma_{com}\hat{\tau} = 0.02$). (a) Structure factor of the three systems for three different system sizes in log–log scale. The dashed line represents a power law scaling of k^{-2}. The inset is the same plot for the static velocity factor. (b) Value of the plateau of the MSD of the three systems as a function of the number of particles, averaged over five different realizations in semi-log. The dashed line is a fit of the logarithmic increase in the equilibrium curve. (c) Translational correlation function of the three systems as a function of the distance in log–log scale with $N = 440\,538$. The dashed line corresponds to the expected power law scaling of g_G extracted from the logarithmic increase in the equilibrium curve in (b).

investigations. The large time MSD of the Δ model displays two distinct logarithmic increases corresponding to the two plateaus reached at large and low k by the structure factor. While the mechanism behind this double logarithmic scaling differs from the one arising due to the difference of temperature between a global and a local COM conserving bath in Eq. (15) (here, we recall that there is no global bath since $\gamma_{com} = 0$), the mathematics remain the same, as the low-k structure factor is related to the SDF and, consequently, the MSD through Eq. (17). At small wavectors, we conclude that any 2D isotropic harmonic crystal displaying a hyperuniform scaling in $k \in [k_1, k_2]$ and otherwise a constant structure factor, will exhibit this double logarithmic scaling on the displacement correlation; one in the region $r \gg 2\pi/k_1$ and one in $r \ll 2\pi/k_2$ with a transition region in between. $S(k \to 0)$ and $S(k \to \infty)$ will be proportional to the prefactor of the long and short range logarithmic increase in the MSD, respectively. If the hyperuniformity extends to $k_1 = 0$, the plateau of the MSD eventually reaches a constant. The translational correlation function of the Δ model also exhibits a double power law decrease, in line with the double logarithmic increase in the plateau of the MSD. The system displays a quasi-long-range order as well.

Finally, by introducing a global damping $\gamma_{com} \neq 0$ to the Δ model, but still with $T_{com} = 0$, we obtain the "$\Delta + \gamma_{com}$" system, which exhibits hyperuniformity on large length scales with a power law consistent with $S(k) \sim k^2$, as predicted in Eq. (13). From the static velocity factor, we confirm that the energy is not evenly distributed across scales but concentrated at fine ones and depleted at larger ones with a k^2 power law decrease. From the MSD, we observe an initial logarithmic increase, followed by a plateau, in line with Eq. (16) when $T_{com} = 0$. This implies the reaching of a constant value for the correlation function at large distances, which is the hallmark of a translational long-range order and the breakdown of the HMW theorem, as expected when the COM is conserved in the presence of global damping.

C. Arbitrary enhancement of quasi-long-range order via non-equilibrium effects

We now turn to analysis of our full system with $T_{com} \neq 0$ and will show that the relevant temperature is, as expected from the theory, the temperature of the COM and not the temperature of the system T or the temperature of the active collisions T_{loc}. The results for a range of temperatures T_{com} of the global bath are shown in Fig. 3(a). In the main figure, we show various curves of the plateau of the MSD vs the number of particles in the system N for different T_{com} in a semi-log scale. We also provide results for the structure factor and translational pair correlation function in the presence of global bath in Appendix H. We ensure N is sufficiently large to only observe the MSD scaling associated with the COM temperature. As expected from Eq. (15), the increase in the MSD is logarithmic and is greater the larger is T_{com}. Of course, we recover a true long-range order in the limit $T_{com} \to 0$ with a flat plateau of the MSD. In the inset, we extract the coefficient κ in front of the logarithmic increase in the MSD as a function of T_{com}. That is,

$$\mathrm{MSD}_{T_{com}}(t \to \infty) = \kappa(T_{com}) \log(N). \tag{25}$$

This quantity could have equivalently been obtained from the exponent of the correlation function or from $S(0)$.

For a harmonic crystal, κ corresponds, up to a constant factor, to the exponent of the power law decay of the translational correlation function [see Eqs. (15) and (16)] and is given by

$$\kappa \sim T_{com}/K. \tag{26}$$

However, this simple linear increase in κ with T_{com} holds only for harmonic crystals, not for a crystal of active hard disks. The elastic modulus of an equilibrium hard-disk crystal scales trivially with the temperature of the system T,[112–114]

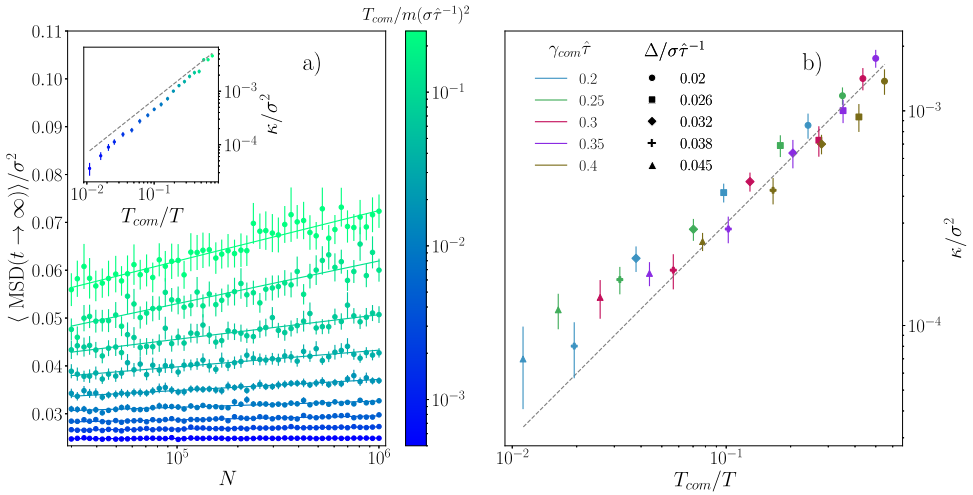

FIG. 3. Quasi-long-range order dependence on COM temperature. (a) Simulation of a system of active hard disks at fixed $\Delta/\sigma\hat{\tau}^{-1} = 0.04$, $\gamma_{com}\hat{\tau} = 0.3$, and $\alpha = 0.95$ for different values of the global Langevin bath temperature T_{com} at fixed γ_{com}. We assume that T_{loc} is fixed and given by Eq. (G2). The main figure shows the dependence on T_{com} of the plateau of the MSD for various system sizes. T is the kinetic energy of the system [see Eq. (20)]. The coefficient in front of the logarithmic increase in the MSD κ is shown in the inset as a function of T_{com}/T. A linear scaling is represented by the gray dashed line as a guide. (b) Scaling of the logarithmic increase in the MSD for multiple systems with various Δ and γ_{com} at fixed $T_{com}/m(\sigma\hat{\tau}^{-1})^2 = 0.0025$. The underlying finite size analysis on the MSD is performed for 30 systems ranging from $N = 29\,946$ to $N = 1\,000\,680$ for each point. A linear scaling is represented by the gray dashed line as a guide.

$$K(T) = \tilde{K}T. \tag{27}$$

This implies that the scaling of the MSD of an equilibrium hard-disk system is not expected to grow with the temperature since $T_{com} = T$. While our system is a non-equilibrium hard-disk solid, we make the assumption that Eq. (27) is still a good approximation for the effective elastic constant, thus predicting the following scaling:

$$\kappa \sim \frac{T_{com}}{T}. \tag{28}$$

This scaling is well verified in our case, as shown in the inset of Fig. 3, where the dashed line represents a linear increase in κ with T_{com}/T.

In panel (b), we performed the same simulations as for panel (a), except that we varied Δ and γ_{com} at fixed T_{com}. We observe again approximately a linear scaling of κ as a function of T_{com}/T, implying that the effective constant of the lattice was roughly constant.

These two analyses indicate that, as predicted from the theory, for active hard sphere crystals, the relevant parameter to manipulate in order to slow down the decay of the translational quasi-long-range is T_{com}/T. Counterintuitively, this implies that increasing the kinetic energy of the system at a fixed center of mass temperature increases the quasi-long-range order. Indeed, we can obtain the same enhancement of the quasi-long-range order given by the reduction of T_{com} by keeping it fixed while varying the driving and dissipative parameters Δ and γ_{com}.

IV. CONCLUSIONS AND PERSPECTIVES TOWARD REALISTIC SYSTEMS

In this paper, we studied the Hohenberg–Mermin–Wagner theorem's applicability to non-equilibrium systems. By examining a theoretical model of a harmonic crystal coupled to a local and a global thermal-like bath, we find that the translational long-range order is controlled by the temperature of the center of mass, rather than the overall kinetic energy, as in equilibrium systems. This result also offers a way to better rationalize the violation of the HMW theorem observed in the random organization model[33] via a k-dependent temperature. Moreover, through numerical simulations of a hard-disk solid driven out-of-equilibrium by active collisions, we showed the possibility to suppress density fluctuations and enhance the quasi-long-range translational order without neglecting or fine-tuning thermal fluctuations. These insights provide a valuable theoretical understanding of crystalline phases in non-equilibrium systems.

To conclude, we outline a possible application of our results to suppress density fluctuations in a realistic granular system. From the analysis provided in the previous sections, it is clear that an equilibrium-like global thermal noise prevents long-range translational order and hyperuniformity in both the harmonic and the hard-disk driven solid. In these systems, only the exponent of the power-law decay of the correlation function can be tuned. However, true hyperuniformity or equivalently long-range order are unachievable. One might be tempted to think that athermal systems, where the effects of thermal fluctuations are negligible, could provide a suitable playground for the actual realization of a two-dimensional long-range ordered crystal. However, things are not so simple. Indeed, once global thermal fluctuations are neglected, it remains practically very difficult to realize a COM-preserving athermal driving mechanism. Moreover, the effect of any confinement will inevitably influence the COM dynamics. Once this intrinsic difficulty in realizing a true long-range order is accepted, one could still hope to find a way to arbitrarily enhance the quasi-long-range order of a system by tuning some experimental parameters

following a methodology similar to that used for the simulation of the coarse-grained model in Sec. III.

Quasi-2D vibrated granular fluids[38,115–122] represent the realization of the coarse grained model discussed in Sec. III. In these systems, macroscopic grains are confined in a box of size $L \times L \times h$ with $h \ll L$ the height of the box. The box is sinusoidally vibrated, which imparts vertical energy to the grains. Collisions between particles transfer this vertical energy to the xy components of the velocity. Moreover, tangential friction, resulting from collisions with the top or bottom plates, slows down the beads in the xy plane. When viewed purely in the xy plane, this system behaves similarly to the coarse-grained model discussed in Sec. III. Indeed, collisions between particles inject energy into the xy plane and play the same role as Δ in Eq. (23), while the damping γ_{com} during the free flight in the coarse-grained model is equivalent to the energy loss due to collisions with the roof and the bottom plate in the quasi-2D system. Moreover, the roughness of the two horizontal confining plates implies that each grain-plate collision introduces some randomness to the velocities (without even considering the angular momentum of the grains). Remarkably, this effect has been found to act as a small homogeneous thermal noise,[42] which can be mapped into an effective global temperature T_{com}. The fact that this realistic setup is correctly described by the coarse grain model suggests the possibility of enhancing the quasi-long-range order by tuning the experimental parameters (driving amplitude, frequency, material properties, ...) to reduce, as much as possible, the ratio between the effective T_{com} caused by the plate roughness and the horizontal kinetic energy of the system T. Of course, the specific way in which the experimental parameters influence T_{com} and T can be very complex, but after some preliminary analysis, one might, in principle, be able to find the right combination of them to vary in order to arbitrarily reduce T_{com}/T. We look forward to applying these ideas to realistic granular quasi-2D systems in future studies.

ACKNOWLEDGMENTS

We thank Giuseppe Foffi and Frank Smallenburg for carefully reading and commenting on the manuscript. We also thank Andrea Puglisi and Lorenzo Caprini for fruitful scientific discussions. This work has been done with the support of Investissements d'Avenir of LabEx PALM (Grant No. ANR-10-LABX-0039-PALM).

AUTHOR DECLARATIONS

Conflict of Interest

The authors have no conflicts to disclose.

Author Contributions

R. Maire: Conceptualization (equal); Data curation (lead); Formal analysis (lead); Investigation (lead); Methodology (lead); Software (lead); Writing – original draft (lead); Writing – review & editing (lead). **A. Plati**: Conceptualization (equal); Data curation (supporting); Formal analysis (supporting); Investigation (supporting); Methodology (supporting); Software (supporting); Supervision (lead); Writing – original draft (supporting); Writing – review & editing (supporting).

DATA AVAILABILITY

The data that support the findings of this study are available from the corresponding author upon reasonable request.

APPENDIX A: DISCRETE REAL-SPACE CONSERVING NOISES FOR VECTORIAL QUANTITIES

In Sec. II, we introduced a momentum conserving noise. On a general lattice, such noise can be written as

$$m\ddot{\boldsymbol{u}}_n = -\gamma_{loc}\Lambda(\dot{\boldsymbol{u}}_n) + \sqrt{2\gamma_{loc}T_{loc}}(\nabla \cdot \boldsymbol{\Xi}_n). \tag{A1}$$

The first term is a discrete Laplacian and the second is a discrete divergence of a rank 2 random tensor. Once the discrete differential operators are well defined, this equation can be understood as a discrete analog of the model B field theory,

$$m\ddot{\boldsymbol{u}}_n = -\gamma_{loc}\nabla \cdot (\nabla\dot{\boldsymbol{u}}_n + \sqrt{2\gamma_{loc}T_{loc}}\boldsymbol{\Xi}_n), \tag{A2}$$

with ∇ a discrete gradient operator. Under this form, $\boldsymbol{\Xi}$ is immediately interpreted as a flux of momentum. However, it should be noted that the global conservation of momentum depends on boundary conditions.

On a general basis, any lattice can be understood as a graph $\mathcal{G}$ with a set of vertices $\mathcal{V}$ and edges $\mathcal{E}$ connecting them. The usual notion of continuous field living on $\mathbb{R}^d$ (or more generally on a manifold) is replaced by the notion of field living on vertices and mapping vertex to vectors. For example, in our case, $\boldsymbol{u} : \mathcal{V} \to \mathbb{R}^2$. The complexity of dealing with discrete calculus on lattices lies in the fact that the discrete gradient maps fields living on vertices to fields living on the edges, while the discrete divergence maps fields living on the edges to fields living on the vertices.[123,124] Hence, the Laplacian being the composition of the divergence with the gradient maps fields leaving on the vertices to fields living on the vertices. This immediately implies that the divergence in Eq. (A1) is ill-defined if the random tensor $\boldsymbol{\Xi}$ lives on the vertices and not on the edges. Following Ref. 68, we will see that this term can be represented through a finite difference of random vertices field. Moreover, in order for the dynamics to be equilibrium-like, the discretization scheme of the differential operators and the variance of the noise must be well chosen in order to respect the FDT.

Indeed, if we start from a definition of the derivative as a finite difference of terms, we can write the divergence of a tensor $\nabla \cdot \boldsymbol{a}_n$ as finite differences between neighboring points. Then, the corresponding discrete Laplacian Λ takes the form $\Lambda(\boldsymbol{a}_n) = \nabla \cdot (\nabla \boldsymbol{a}_n)$ where ∇ is a gradient defined from the chosen finite difference used for the derivative. With these choices, taking $\boldsymbol{\Xi}$ with a unit variance leads to dynamics that correctly respects the FDT.

As an example, if we define the derivative on a square lattice as the forward finite difference, then

$$\nabla \cdot \boldsymbol{\Xi}_{i,j} = \begin{pmatrix} \Xi^{x,x}_{i+1,j} - \Xi^{x,x}_{i,j} + \Xi^{x,y}_{i,j+1} - \Xi^{x,y}_{i,j} \\ \Xi^{y,x}_{i+1,j} - \Xi^{y,x}_{i,j} + \Xi^{y,y}_{i,j+1} - \Xi^{y,y}_{i,j} \end{pmatrix}, \tag{A3}$$

where we replaced the usual lower vectorial index n by two indices i and j, denoting the x and y position on the lattice. Then, we can check that if $\boldsymbol{\Xi}$ has a unit variance,

$$\langle \Xi^{\alpha,\mu}_{i,j}(t)\Xi^{\beta,\nu}_{k,l}(t')\rangle = \delta(t'-t)\delta^{\alpha,\beta}\delta^{\mu,\nu}\delta_{i,k}\delta_{j,l}, \tag{A4}$$

then

$$\langle(\nabla\cdot\Xi_{i,j}(t))^{\alpha}(\nabla\cdot\Xi_{k,l}(t'))^{\beta}\rangle = \delta^{\alpha,\beta}\delta(t-t')\big(4\delta_{i,k}\delta_{j,l} - \delta_{i+1,k}\delta_{j,l} - \delta_{i,k}\delta_{j+1,l} - \delta_{i-1,k}\delta_{j,l} - \delta_{i,k}\delta_{j-1,l}\big), \quad \text{(A5)}$$

where we recognize the discrete Laplacian found for simple forward finite differences, a sum over first neighbors. A different discretization of the derivative [Eq. (A3)] would have given us a different correlation corresponding to the adequate Laplacian to use in order for the system to respect the FDT. For example, a symmetric representation of the derivative would have given rise to a Laplacian with second neighbors.[48] Conservative discrete equations in real space have been used in a plethora of domains[48,51,68,125,126] and naturally arise when a stochastic partial differential equation is discretized to be solved numerically.

APPENDIX B: FOURIER TRANSFORM CONVENTION

We choose the following convention for the semi-discrete Fourier transform:

$$\tilde{f}_k(w) = \int_{-\infty}^{\infty} \mathrm{d}t \frac{1}{N}\sum_{\boldsymbol{n}} e^{iwt+ik\cdot n} f_n(t),$$
$$f_n(t) = \frac{1}{(2\pi)^3}\int_{-\infty}^{\infty} dw \frac{1}{N}\sum_{\boldsymbol{k}} e^{-iwt-i\boldsymbol{k}\cdot\boldsymbol{n}}\tilde{f}_k(w), \quad \text{(B1)}$$

with $\boldsymbol{k} = 2\pi\boldsymbol{n}/L$ and $n^{\alpha} \in -\sqrt{N}/2+1,\ldots,\sqrt{N}/2$. When the spatial continuous limit is taken, we obtain the following Fourier series representation of the real lattice:

$$f_n(t) = \frac{1}{(2\pi)^3}\int_{-\infty}^{\infty} dw \frac{a^2}{(2\pi)^2}\int_{-\pi/a}^{\pi/a} \mathrm{d}\boldsymbol{k} e^{-iwt-i\boldsymbol{k}\cdot\boldsymbol{n}}\tilde{f}(\boldsymbol{k},w). \quad \text{(B2)}$$

This follows directly from taking the limit $a \to 0$ while keeping L fixed (or $L \to \infty$ at fixed $L/\sqrt{N} = a$) and corresponds to an integration in the first Brillouin zone.

APPENDIX C: ANHARMONIC LATTICES

The theory described in Sec. II was developed with respect to an harmonic lattice. While anharmonicity leads to benign effects such as renormalization of the harmonic spring constant, it also leads to energy transfer between modes, which could change the phenomenology found for a harmonic lattice. In this section, we argue that this is not the case.

In a system with anharmonic interaction, each mode would still be driven at temperature $\tilde{T}_k$ as in the harmonic case; however, a transfer of energy between them would be observed. We can take, as an example, simple polynomial forces in real space (without loss of generality, we will stay in 1D; see Ref. 127 for a generalization in higher dimension),

$$F_{\text{anharmonic}} = -\sum_{b=2}^{\infty}\beta_b\sum_{\{\tilde{n}\}}(u_n - u_{\tilde{n}})|u_n - u_{\tilde{n}}|^{b-1},$$

with β_b being coupling constants and b the power law exponent associated with the anharmonic term. In Fourier space for the mode k, such force is written as[128]

$$F_{\text{anharmonic}} = -\sum_{b=2}^{\infty}\beta_b\sum_{k_1,k_2,\ldots,k_b} V_b^{k,k_1,k_2,\ldots,k_b} \times \tilde{u}_{k_1}\tilde{u}_{k_2}\ldots\tilde{u}_{k_b}\delta_{k+k_1+k_2+\cdot s+k_b}. \quad \text{(C1)}$$

The Kronecker δ ensures that the momentum is conserved by the scattering of waves. Here, $\beta_b V_b^{k,k_1,k_2,\ldots,k_b}$ is the interaction strength of a scattering due to the anharmonicity with power b. Such equations are common in wave turbulence.[129] For nearest neighbor interaction in 1D, we can show that

$$V_b^{k,k_1,k_2,\ldots,k_b} \propto \sin(ka/2)\sin(k_1a/2)\ldots\sin(k_ab/2), \quad \text{(C2)}$$

with a being the lattice spacing. These equations are making clear the fact that, with anharmonic terms, modes interact.

A proof of the absence of long-range order in systems with anharmonic interactions is beyond the scope of this work and would most likely require the full stationary distribution to be known, as in the equilibrium case.[2] For example, the steady-state distribution of a three-body system, with each particle driven at a different temperature and interacting through a harmonic potential, is known but already shows great complexity.[68] However, a qualitative argument can be made, suggesting that the overall picture presented in this section should remain largely unaffected at large length scales even in the presence of anharmonic interactions.

Since the energy is created at the level of collision $k \simeq 2\pi/a$, the most excited modes will be those around this length scale. The following question remains to be answered: can these modes transfer energy sufficiently quickly to the modes at $k \to 0$ so that very large wavelength phonons are excited and can reach a non-vanishing temperature? The interaction strength between these two scales is given by $V_b^{k\simeq 0,k_1,\ldots,k_m\simeq 2\pi/a,\ldots,k_b}$ where at least one of the mode is close to 0 (long wavelength) and one mode is close to $2\pi/a$ (collisional/energy creation length scale). However, from Eq. (C2), it is clear that the strength of such a process goes to 0 with $k \to 0$. Hence, the rate of energy transfer to modes with very large wavelength is vanishingly small with k. Since the continuous damping effectively dissipates any energy supplied to these modes on a timescale by γ_{com}, the phenomenology observed for the harmonic case is expected to hold qualitatively. That is, we expect the low-k mode to roughly be at temperature $\tilde{T}_k$, with $T_{k\to 0} = 0$. It should be noted that the argument holds in larger dimensions where the exact expression $V_b^{\boldsymbol{k},\boldsymbol{k}_1,\boldsymbol{k}_2,\ldots,\boldsymbol{k}_b}$ contains a term similar to the dispersion relation for each mode k, which vanishes when $k \to 0$.

APPENDIX D: COMPUTATION OF THE DISPLACEMENT CORRELATION FUNCTION

The displacement correlation function is computed in the infinite size limit where the discrete Fourier transform over wavevectors is approximated as a continuous Fourier transform (see Appendix B),

$$\langle(\boldsymbol{u}_n-\boldsymbol{u}_m)^2\rangle = \frac{a^4}{(2\pi)^4}\int \mathrm{d}\boldsymbol{k}\mathrm{d}\boldsymbol{q}(e^{ia\boldsymbol{k}\cdot\boldsymbol{n}}-e^{ia\boldsymbol{k}\cdot\boldsymbol{m}}) \times (e^{ia\boldsymbol{q}\cdot\boldsymbol{n}}-e^{ia\boldsymbol{q}\cdot\boldsymbol{m}})\langle\tilde{\boldsymbol{u}}(k,t=0)\tilde{\boldsymbol{u}}(q,t=0)\rangle = \frac{a^2}{2\pi^2}\int \mathrm{d}\boldsymbol{k}(1-\cos(a\boldsymbol{k}\cdot(\boldsymbol{n}-\boldsymbol{m}))C_{uu}(\boldsymbol{k}). \quad \text{(D1)}$$

Since we only are interested in the (quasi-)long-range behavior of our system, we compute the long distance limit of this object. We decompose the integral into two intervals. From 0 to $1/a|\boldsymbol{n}-\boldsymbol{m}|$, if $T_{com}\neq 0$, the integral is bounded by a term in $1/\omega_k^2$ and can be neglected. For the second interval from $1/a|\boldsymbol{n}-\boldsymbol{m}|$ to $2\pi/a$, the oscillating part averages out. Similar arguments work for $T_{com}=0$. Up to a constant, at long distances, Eq. (D1) is thus approximated as

$$\begin{aligned}\langle(\boldsymbol{u}_n-\boldsymbol{u}_m)^2\rangle &\simeq \frac{a^2}{\pi}\int_{\frac{1}{a|\boldsymbol{n}-\boldsymbol{m}|}}^{\frac{\pi}{a}}\mathrm{d}kC_{uu}(k)k \\ &\simeq \Bigg[(T-T_{com})\log\frac{\gamma_{com}/\gamma+\pi^2}{\gamma_{com}/\gamma+1/|\boldsymbol{n}-\boldsymbol{m}|^2} + 2T_{com}\log(\pi|\boldsymbol{n}-\boldsymbol{m}|)\Bigg]/\pi K \\ &\simeq \begin{cases}\dfrac{2T_{com}}{\pi K}\log(\pi|\boldsymbol{n}-\boldsymbol{m}|) & |\boldsymbol{n}-\boldsymbol{m}|\gg\delta^{-1},\\ \dfrac{2T_{loc}}{\pi K}\log(\pi|\boldsymbol{n}-\boldsymbol{m}|)) & |\boldsymbol{n}-\boldsymbol{m}|\ll\delta^{-1}.\end{cases}\end{aligned} \quad \text{(D2)}$$

which gives Eq. (15).

APPENDIX E: ENTROPONS IN A TWO TEMPERATURE DELTA CORRELATED BATH

Entropons, as discussed in the recent work by Caprini *et al.*,[69,97] are general non-equilibrium collective excitations linked to the spectral entropy production and are a consequence of a Harada–Sasa-like relation.[48,97,130] Indeed, for a generalized Langevin equation,

$$\ddot{\tilde{u}}_k(t) = -K\omega_k^2\tilde{u}_k - \int_{-\infty}^{\infty}\mathrm{d}t'\Gamma(k,t-t')\dot{\tilde{u}}_k(t') + F + \tilde{\mathcal{E}}_k(t), \quad \text{(E1)}$$

with $\Gamma(t)$ the friction kernel and $\langle\tilde{\mathcal{E}}_k(t')\tilde{\mathcal{E}}_q(t)\rangle = \tilde{\nu}(k,t-t')\delta_{k,-q}$, we can prove that if the force F is even under time reversal, the following relation holds:[131]

$$\frac{C_{uu}(k,w)}{\nu(k,w)} = \frac{\Im(R(k,w))}{w\Re(\Gamma(k,w))} + \frac{\sigma^g(k,w)}{2\Re(\Gamma(k,w))^2w^2}, \quad \text{(E2)}$$

where

$$\sigma^g(k,w) = 2\Im\langle\tilde{u}(k,w)F(-k,-w)\rangle\Re(\Gamma(k,w))\nu^{-1}(k,w)w \quad \text{(E3)}$$

is the entropy production of the generalized Langevin equation and $R(\mathbf{k},w)$ is the response of the displacement to an instantaneous force, while $\Re$ and $\Im$ are the real and imaginary parts, respectively, of the function in front of it. It should be noted that this formula holds independently on the choice of the noise correlation and damping. Notably, in the case that we are interested, $\Gamma(k,w)=\gamma_{com}+\gamma_{loc}\omega_k^2$ and $\nu(w)/\Gamma(k,w)=2\tilde{T}_k$, without additional forces, the spectral entropy production σ^g is equal to 0, and the non-equilibrium character of the system is only included in the effective temperature $T_{\text{eff}}(k,w)=\nu(k,w)/(2\Gamma(k,w))$. In this sense, we might consider that entropons are absent, and only phonons at an effective temperature exist in our system since the dynamic SDF reads

$$C_{uu}(k,w) = \frac{2\tilde{T}_k}{w}\Im(R(k,w)). \quad \text{(E4)}$$

The entropy production equal to 0 might come as a surprise since it is clear that as long as $T_{com}\neq T_{loc}$, heat flows from one reservoir to another, and thus, entropy is continuously created. However, the particle itself is oblivious to these heat transfers between baths because they collectively act as a unique equilibrium-like reservoir with an effective temperature and viscosity.[132–134] From the point of view of the particle, the system is thus too coarse-grained to probe these non-equilibrium effects, and heat fluxes between reservoirs are invisible to dynamical observables.[135,136]

To circumvent this issue, we can rewrite our model in an equivalent form for the particle, with an auxiliary variable.[136–144] This auxiliary variable provides enough information about the system to probe the heat fluxes between reservoirs and compute the spectral heat flow between them. The heat flux for Eq. (6) is given by[137]

$$m\dot{Q}(k,w) = \frac{4\gamma_{com}\gamma_{loc}\omega_k^2(T_{com}-T_{loc})w^2}{(K\omega_k^2-mw^2)^2+(\gamma_{com}+\gamma_{loc}\omega_k^2)^2w^2}. \quad \text{(E5)}$$

From which, we can prove in our system without additional forces that

$$C_{uu}(k,w) = \frac{2T_{loc}}{w}\Im(R(k,w)) + \frac{1}{2w^2\gamma_{loc}\omega_k^2}\dot{Q}(k,w) \quad \text{(E6)}$$

or

$$C_{uu}(k,w) = \frac{2T_{com}}{w}\Im(R(k,w)) - \frac{1}{2w^2\gamma_{com}}\dot{Q}(k,w). \quad \text{(E7)}$$

The first term represents the usual equilibrium phonons at temperature T_{loc}, while the second term is clearly a non-equilibrium term, vanishing when $T_{com}=T_{loc}$ and proportional to the heat transferred between reservoirs. This new term, arising from a rewriting of the effective temperature is very similar to entropons, except that it is better written as proportional to the heat transfer instead of the entropy production due to Fourier's law. However, it should be noted that, contrary to entropons arising from active forces, this new term might be negative according to which bath we chose as the one with the reference temperature in front of the linear response function.

The equivalence between Eqs. (E6) and (E7) and Eq. (E4) can be proved more generally with multiple exponentially correlated reservoirs and external non-conservative forces using the Markovian auxiliary variable representation of the generalized Langevin equation. Hence, for non-interacting systems, the effective temperature in the $\boldsymbol{k},w$ space, obtained from the ratio between the autocorrelation and the response function, can be expressed as the temperature of a bath plus terms proportional to the heat flow between all the other baths. We look forward to developing these ideas in future work.

APPENDIX F: HYBRID EVENT-DRIVEN/TIME-STEPPED MOLECULAR DYNAMICS

Since the potential of hard-disk particles is discontinuous, usual time-stepped molecular dynamics methods are not suitable for the simulations of such systems. Instead, we use event-driven methods,[108] where the time before the collision of two particles i and j denoted by t_{ij}^{col}, can be analytically computed,

$$|\boldsymbol{r}_i(t_{ij}^{col}) + \boldsymbol{r}_j(t_{ij}^{col})| = \frac{\sigma_i + \sigma_j}{2}, \tag{F1}$$

with $r_i(t)$ being the position of particle i at time t. For particles free flying or undergoing constant viscous drag, t_{col}^{ij} can be found exactly from the initial velocities and positions of the particles.

For viscous friction, the time before the next collision is

$$t_{ij}^{col} = -\log(1 - \gamma_{com}\delta t_{ij})/\gamma_{com}, \tag{F2}$$

with

$$\delta t_{ij} = \frac{-b - \sqrt{b^2 - \boldsymbol{v}_{ij}^2(\boldsymbol{r}_{ij}^2 - (\sigma_i + \sigma_j)^2/4)}}{\boldsymbol{v}_{ij}^2}, \tag{F3}$$

where $b = \boldsymbol{r}_{ij} \cdot \boldsymbol{v}_{ij}$ and $\boldsymbol{r}_{ij}$ and $\boldsymbol{v}_{ij}$ are the relative position and velocity of particles i and j , respectively, at the moment the subsequent collision time is computed. From every collision time and the collision rule (23), the full dynamics of the system can be solved exactly in the absence of T_{com}. When the bath has a non-zero temperature, we must include the effect of the thermostat in the system by adding events every δt_{noise} where each particle is kicked by an amount $\sqrt{2\gamma_{com}T_{com}\delta t_{noise}}/m$. The FDT is respected for every value of δt_{noise} because of the continuous nature of the damping.[145] Nonetheless, we chose $\delta t_{noise} \ll \tau_f \equiv 1/\omega(\phi, T)$ the mean free time.

APPENDIX G: TEMPERATURE OF THE ACTIVE COLLISION BATH

For the model including only active collisions ($\gamma_{com} = 0$), the average energy change during a collision can be obtained from the collision rule (24),

$$\langle E' - E\rangle_{coll} = m\Delta^2 + m\alpha\Delta\langle|\boldsymbol{v}_{ij}\cdot\hat{\boldsymbol{\sigma}}_{ij}|\rangle_{coll} - m\frac{1-\alpha^2}{4}\langle|\boldsymbol{v}_{ij}\cdot\hat{\boldsymbol{\sigma}}_{ij}|^2\rangle_{coll}, \tag{G1}$$

where the average can be computed from the assumption of molecular chaos, Gaussianity, and using the cross section of hard disks.[38,106,146] In the steady state, on average collisions do not inject or retrieve energy from the system. The steady-state temperature T_{loc} is thus given by the zero of Eq. (G1), which is[106]

$$T_{loc} = \Delta^2\left(\frac{\epsilon + \sqrt{\epsilon^2 + 4m(1-\alpha^2)}}{2(1-\alpha^2)}\right)^2, \tag{G2}$$

with $\epsilon = \alpha\sqrt{\pi m}$. This can be taken as the temperature T_{loc} of the local bath. It can be shown[38] that when damping is added to the system, far from the absorbing state, the new temperature of the system T keeps the exact same form as Eq. (G2) but with $\epsilon = \alpha\sqrt{\pi m} - \gamma_{com}\sigma\sqrt{\pi m}/2\Delta\phi\chi(\phi)$, with $\chi(\phi)$ the radial distribution function at contact.

This implies that the temperature of the system T does not behave as the temperature of a system subject to a Langevin bath at temperature T_{loc} and damping$\gamma_{loc}\omega_\kappa^2$ on top of which, we add an additional damping γ_{com}. This is due to the dependence of Eq. (G1) on the relative velocity of particles at collision, which indicates that T_{loc} should itself be dependent on the other sources of energy change

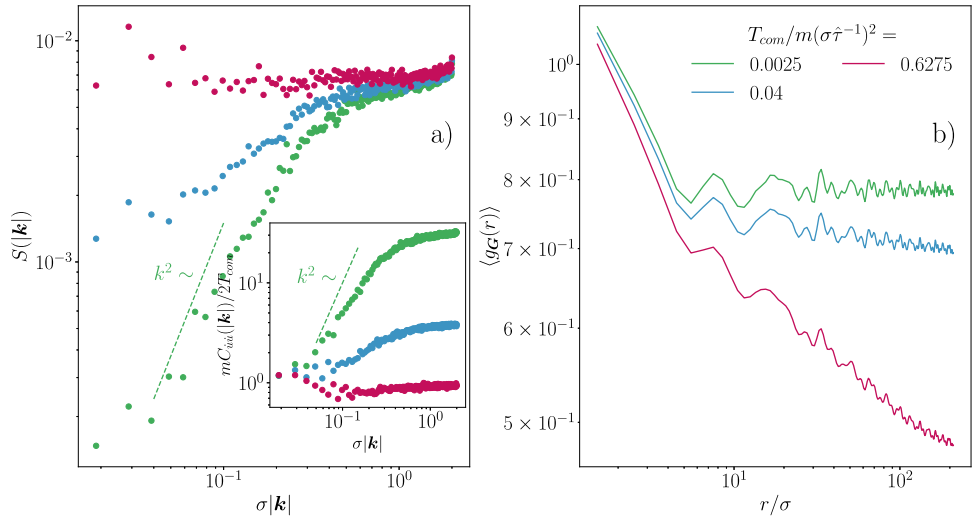

FIG. 4. Effect of a global bath on the $\Delta + \gamma$ model for the structure factor and the translational pair correlation function. (a) Main figure: structure factor as a function of the wavenumber. For lower T_{com}, it is easier to observe a transient hyperuniform scaling k^2. In the limit $T_{com} = 0$, the hyperuniform scaling continues to $k = 0$. Inset: static velocity factor divided by T_{com} as a function of k. We obtain the limit $mC_{\dot{u}\dot{u}}(|\boldsymbol{k}| \to 0)/2 = T_{com}$ as expected from $T_{k\to 0} = T_{com}$. (b) Translational correlation function as a function of r. With increasing T_{com}, we observe a stronger quasi-long-range power law decay. In the limit $T_{com} = 0$, g_G flattens and true long-range order is obtained. $N = 500\,080$, $\phi = 0.765$, $\Delta/\sigma\hat{\tau}^{-1} = 0.04$, $\gamma_{com}\hat{\tau} = 0.3$, and $\alpha = 0.95$.

in the system. It will not cause any significant practical problem, but this is a peculiarity that should be kept in mind.

APPENDIX H: STRUCTURE FACTOR AND TRANSLATIONAL CORRELATION FUNCTION IN THE PRESENCE OF A GLOBAL BATH

In Fig. 3, we analyzed the dependence of the MSD on T_{com}. As shown in Fig. 2 and described in the theory, the plateau of the MSD, the low-k structure factor, and the long-range behavior of the translational pair correlation function contain the same information as given by Eqs. (14) and (17). Nonetheless, as a consistent check, it is interesting to numerically confirm these predictions in our active hard disk model. In Fig. 4(a), we show the structure factor of systems driven at different global bath temperatures. As expected, we observe that the smaller T_{com} is, the lower the structure factor can go, in agreement with Eq. (13). The increase in the plateau of the MSD with system size is proportional to $S(0)$; however, in the main text, we use the MSD since we consider it to provide better data for finite system size (at infinite system size, it would be easier to measure the plateau of the structure factor at low k). In the inset, we also provide the velocity static factor that converges, as it should for small k to $T_{k\to 0} = T_{com}$. In Fig. 4(b), we show the translational pair correlation for these systems. Their long-range behavior is in agreement with Eq. (16): they exhibit a power law decay with an exponent increasing with T_{com}. The exponent of the power law decay is proportional to the increase in the MSD plateau; however, as for the structure factor, data are cleaner with the MSD.

REFERENCES

[1] P. C. Hohenberg, "Existence of long-range order in one and two dimensions," Phys. Rev. **158**(2), 383 (1967).
[2] N. David Mermin and H. Wagner, "Absence of ferromagnetism or antiferromagnetism in one- or two-dimensional isotropic Heisenberg models," Phys. Rev. Lett. **17**(22), 1133 (1966).
[3] B. I. Halperin, "On the Hohenberg–Mermin–Wagner theorem and its limitations," J. Stat. Phys. **175**(3–4), 521–529 (2019).
[4] N. D. Mermin, "Crystalline order in two dimensions," Phys. Rev. **176**(1), 250 (1968).
[5] B. Julian Alder and T. E. Wainwright, "Phase transition for a hard sphere system," J. Chem. Phys. **27**(5), 1208–1209 (1957).
[6] J. Fröhlich and C. Pfister, "On the absence of spontaneous symmetry breaking and of crystalline ordering in two-dimensional systems," Commun. Math. Phys. **81**, 277–298 (1981).
[7] D. R. Nelson and K. J. Strandburg, *Bond-Orientational Order in Condensed Matter Systems*, *Partially Ordered Systems* (Springer, New York, 2012).
[8] U. Gasser, "Crystallization in three- and two-dimensional colloidal suspensions," J. Phys.: Condens. Matter **21**(20), 203101 (2009).
[9] A. Cavagna, A. Cimarelli, I. Giardina, G. Parisi, R. Santagati, F. Stefanini, and M. Viale, "Scale-free correlations in starling flocks," Proc. Natl. Acad. Sci. U. S. A. **107**(26), 11865–11870 (2010).
[10] T. Vicsek, A. Czirók, E. Ben-Jacob, I. Cohen, and O. Shochet, "Novel type of phase transition in a system of self-driven particles," Phys. Rev. Lett. **75**(6), 1226 (1995).
[11] J. Toner and Y. Tu, "Long-range order in a two-dimensional dynamical XY model: How birds fly together," Phys. Rev. Lett. **75**(23), 4326 (1995).
[12] J. Toner and Y. Tu, "Flocks, herds, and schools: A quantitative theory of flocking," Phys. Rev. E **58**(4), 4828 (1998).
[13] J. Toner, Y. Tu, and S. Ramaswamy, "Hydrodynamics and phases of flocks," Ann. Phys. **318**(1), 170–244 (2005).
[14] E. Bertin, M. Droz, and G. Grégoire, "Hydrodynamic equations for self-propelled particles: Microscopic derivation and stability analysis," J. Phys. A: Math. Theor. **42**(44), 445001 (2009).
[15] C. A. Weber, T. Hanke, J. Deseigne, S. Léonard, O. Dauchot, E. Frey, and H. Chaté, "Long-range ordering of vibrated polar disks," Phys. Rev. Lett. **110**(20), 208001 (2013).
[16] K. E. Bassler and Z. Rácz, "Existence of long-range order in the steady state of a two-dimensional, two-temperature *XY* model," Phys. Rev. E **52**(1), R9 (1995).
[17] M. D. Reichl, C. I. Del Genio, and K. E. Bassler, "Phase diagram for a two-dimensional, two-temperature, diffusive *XY* model," Phys. Rev. E **82**(4), 040102 (2010).
[18] L. Giomi, J. Toner, and N. Sarkar, "Long-ranged order and flow alignment in sheared *p*-atic liquid crystals," Phys. Rev. Lett. **129**(6), 067801 (2022).
[19] H. Nakano, Y. Minami, and S.-i. Sasa, "Long-range phase order in two dimensions under shear flow," Phys. Rev. Lett. **126**(16), 160604 (2021).
[20] Y. Minami and H. Nakano, "Origin of long-range order in a two-dimensional nonequilibrium system under laminar flows," arXiv:2212.06390 (2022).
[21] Y. Minami, H. Nakano, and Y. Hidaka, "Rainbow Nambu-Goldstone modes under a shear flow," Phys. Rev. Lett. **126**(14), 141601 (2021).
[22] H. Ikeda, "Scaling theory of continuous symmetry breaking under advection," arXiv:2401.01603 (2024).
[23] H. Ikeda and Y. Kuroda, "Does spontaneous symmetry breaking occur in periodically driven low-dimensional non-equilibrium classical systems?," arXiv:2304.14235 (2023).
[24] H. Ikeda, "Correlated noise and critical dimensions," Phys. Rev. E **108**(6), 064119 (2023).
[25] B. Benvegnen, O. Granek, S. Ro, R. Yaacoby, H. Chaté, Y. Kafri, D. Mukamel, A. Solon, and J. Tailleur, "Metastability of discrete-symmetry flocks," Phys. Rev. Lett. **131**, 218301 (2023).
[26] A. Maitra and S. Ramaswamy, "Oriented active solids," Phys. Rev. Lett. **123**, 238001 (2019).
[27] Q.-L. Lei, M. Pica Ciamarra, and R. Ni, "Nonequilibrium strongly hyperuniform fluids of circle active particles with large local density fluctuations," Sci. Adv. **5**(1), eaau7423 (2019).
[28] C. Huang, L. Chen, and X. Xing, "Alignment destabilizes crystal order in active systems," Phys. Rev. E **104**, 064605 (2021).
[29] X.-q. Shi, F. Cheng, and H. Chaté, "Extreme spontaneous deformations of active crystals," Phys. Rev. Lett. **131**, 108301 (2023).
[30] S. Dey, A. Bhattacharya, and S. Karmakar, "Enhanced long wavelength Mermin-Wagner fluctuations in two-dimensional active crystals and glasses," arXiv:2402.10625 (2024).
[31] S. Ramaswamy, R. A. Simha, and J. Toner, "Active nematics on a substrate: Giant number fluctuations and long-time tails," Europhys. Lett. **62**(2), 196 (2003).
[32] V. Narayan, S. Ramaswamy, and N. Menon, "Long-lived giant number fluctuations in a swarming granular nematic," Science **317**(5834), 105–108 (2007).
[33] L. Galliano, M. E. Cates, and L. Berthier, "Two-dimensional crystals far from equilibrium," Phys. Rev. Lett. **131**, 047101 (2023).
[34] S. Torquato, "Hyperuniform states of matter," Phys. Rep. **745**, 1–95 (2018).
[35] J. Kim and S. Torquato, "Effect of imperfections on the hyperuniformity of many-body systems," Phys. Rev. B **97**(5), 054105 (2018).
[36] Y. Kuroda, T. Kawasaki, and K. Miyazaki, "Long-range translational order and hyperuniformity in two-dimensional chiral active crystal," arXiv:2402.19192 (2024).
[37] Y. Kuroda and K. Miyazaki, "Microscopic theory for hyperuniformity in two-dimensional chiral active fluid," J. Stat. Mech.: Theory Exp. **2023**(10), 103203 (2023).
[38] R. Maire, A. Plati, M. Stockinger, E. Trizac, F. Smallenburg, and G. Foffi, "Interplay between an absorbing phase transition and synchronization in a driven granular system," Phys. Rev. Lett. **132**(23), 238202 (2024).
[39] R. Kubo, "The fluctuation-dissipation theorem," Rep. Prog. Phys. **29**(1), 255 (1966).
[40] U. Marini Bettolo Marconi, A. Puglisi, L. Rondoni, and A. Vulpiani, "Fluctuation–dissipation: Response theory in statistical physics," Phys. Rep. **461**(4-6), 111–195 (2008).

[41] D. Villamaina, A. Baldassarri, A. Puglisi, and A. Vulpiani, "The fluctuation-dissipation relation: How does one compare correlation functions and responses?," J. Stat. Mech.: Theory Exp. **2009**(07), P07024.
[42] A. Puglisi, A. Gnoli, G. Gradenigo, A. Sarracino, and D. Villamaina, "Structure factors in granular experiments with homogeneous fluidization," J. Chem. Phys. **136**(1), 014704 (2012).
[43] E. Mikhailovich Lifshitz and L. Petrovich Pitaevskii, *Statistical Physics: Theory of the Condensed State* (Elsevier, 2013), Vol. 9.
[44] T. P. C. van Noije, M. H. Ernst, E. Trizac, and I. Pagonabarraga, "Randomly driven granular fluids: Large-scale structure," Phys. Rev. E **59**(4), 4326 (1999).
[45] G. Gradenigo, A. Sarracino, D. Villamaina, and A. Puglisi, "Fluctuating hydrodynamics and correlation lengths in a driven granular fluid," J. Stat. Mech.: Theory Exp. **2011**(08), P08017.
[46] U. Marini Bettolo Marconi, L. Caprini, and A. Puglisi, "Hydrodynamics of simple active liquids: The emergence of velocity correlations," New J. Phys. **23**(10), 103024 (2021).
[47] P. C. Hohenberg and B. I. Halperin, "Theory of dynamic critical phenomena," Rev. Mod. Phys. **49**(3), 435 (1977).
[48] C. Nardini, É. Fodor, E. Tjhung, F. van Wijland, J. Tailleur, and M. E. Cates, "Entropy production in field theories without time-reversal symmetry: Quantifying the non-equilibrium character of active matter," Phys. Rev. X **7**(2), 021007 (2017).
[49] U. C. Täuber, "Field-theory approaches to nonequilibrium dynamics," in *Ageing and the Glass Transition* (Springer, 2007), pp. 295–348.
[50] H. Ikeda, "Harmonic chain far from equilibrium: Single-file diffusion, long-range order, and hyperuniformity," arXiv:2309.03155 (2023).
[51] P. Glorioso, J. Guo, J. F. Rodriguez-Nieva, and A. Lucas, "Breakdown of hydrodynamics below four dimensions in a fracton fluid," Nat. Phys. **18**(8), 912–917 (2022).
[52] D. Das, R. Vink, and M. Krüger, "Friction of a driven chain: Role of momentum conservation, goldstone and radiation modes," J. Phys.: Condens. Matter **36**, 215707 (2024).
[53] B. Cui, J. Yang, J. Qiao, M. Jiang, L. Dai, Y.-J. Wang, and A. Zaccone, "Atomic theory of viscoelastic response and memory effects in metallic glasses," Phys. Rev. B **96**(9), 094203 (2017).
[54] A. Plati and A. Puglisi, "Long range correlations and slow time scales in a boundary driven granular model," Sci. Rep. **11**(1), 14206 (2021).
[55] L. Caprini, U. Marini Bettolo Marconi, and A. Puglisi, "Spontaneous velocity alignment in motility-induced phase separation," Phys. Rev. Lett. **124**, 078001 (2020).
[56] P. Espanol and P. B. Warren, "Perspective: Dissipative particle dynamics," J. Chem. Phys. **146**(15), 150901 (2017).
[57] R. D. Groot and P. B. Warren, "Dissipative particle dynamics: Bridging the gap between atomistic and mesoscopic simulation," J. Chem. Phys. **107**(11), 4423–4435 (1997).
[58] C. P. Lowe, "An alternative approach to dissipative particle dynamics," Europhys. Lett. **47**(2), 145 (1999).
[59] A. Castellano, J. P. Batista, and M. J. Verstraete, "Mode-coupling theory of lattice dynamics for classical and quantum crystals," J. Chem. Phys. **159**(23), 234501 (2023).
[60] J. Mabillard and P. Gaspard, "Nonequilibrium statistical mechanics of crystals," J. Stat. Mech.: Theory Exp. **2021**(6), 063207.
[61] K. Hiura, "Microscopic derivation of nonlinear fluctuating hydrodynamics for crystalline solid," Phys. Rev. E **108**, 054101 (2023).
[62] G. Szamel and M. H. Ernst, "Slow modes in crystals: A method to study elastic constants," Phys. Rev. B **48**(1), 112–118 (1993).
[63] G. Szamel, "Statistical mechanics of dissipative transport in crystals," J. Stat. Phys. **87**(5–6), 1067–1082 (1997).
[64] P. D. Fleming and C. Cohen, "Hydrodynamics of solids," Phys. Rev. B **13**(2), 500–516 (1976).
[65] P. C. Martin, O. Parodi, and P. S. Pershan, "Unified hydrodynamic theory for crystals, liquid crystals, and normal fluids," Phys. Rev. A **6**(6), 2401–2420 (1972).
[66] J. Mabillard and P. Gaspard, "Microscopic approach to the macrodynamics of matter with broken symmetries," J. Stat. Mech.: Theory Exp. **2020**(10), 103203; arXiv:2005.14012 [cond-mat].
[67] L. D. Landau, E. M. Lifshitz, R. T. Beyer *et al.*, "Hydrodynamic fluctuations," in *Perspectives in Theoretical Physics* (Elsevier, 1992), pp. 359–361.
[68] A. Cavagna, J. Cristín, I. Giardina, and M. Veca, "From noise on the sites to noise on the links: Discretizing the conserved Kardar-Parisi-Zhang equation in real space," Phys. Rev. E **109**(6), 064136 (2024).
[69] L. Caprini, U. Marini Bettolo Marconi, and H. Löwen, "Entropy production and collective excitations of crystals out of equilibrium: The concept of entropons," Phys. Rev. E **108**(4), 044603 (2023).
[70] P. M. Chaikin and T. C. Lubensky, *Principles of Condensed Matter Physics* (Cambridge University Press, 1995).
[71] J.-P. Hansen and I. R. McDonald, *Theory of Simple Liquids: With Applications to Soft Matter* (Academic Press, 2013).
[72] D. Chen, H. Zhuang, M. Chen, P. Y. Huang, V. Vlcek, and Y. Jiao, "Disordered hyperuniform solid state materials," Appl. Phys. Rev. **10**(2), 021310 (2023).
[73] Q.-L. Lei and R. Ni, "Hydrodynamics of random-organizing hyperuniform fluids," Proc. Natl. Acad. Sci. U. S. A. **116**(46), 22983–22989 (2019).
[74] D. Hexner and D. Levine, "Noise, diffusion, and hyperuniformity," Phys. Rev. Lett. **118**(2), 020601 (2017).
[75] D. Hexner and D. Levine, "Hyperuniformity of critical absorbing states," Phys. Rev. Lett. **114**(11), 110602 (2015).
[76] A. Mukherjee, D. Tapader, A. Hazra, and P. Pradhan, "Anomalous relaxation and hyperuniform fluctuations in center-of-mass conserving systems with broken time-reversal symmetry," arXiv:2312.11181 (2023).
[77] T. Bertrand, D. Chatenay, and R. Voituriez, "Nonlinear diffusion and hyperuniformity from Poisson representation in systems with interaction mediated dynamics," New J. Phys. **21**(12), 123048 (2019).
[78] Y.-W. Li and M. P. Ciamarra, "Accurate determination of the translational correlation function of two-dimensional solids," Phys. Rev. E **100**(6), 062606 (2019).
[79] Y. Imry and L. Gunther, "Fluctuations and physical properties of the two-dimensional crystal lattice," Phys. Rev. B **3**, 3939–3945 (1971).
[80] U. Gasser, C. Eisenmann, G. Maret, and P. Keim, "Melting of crystals in two dimensions," ChemPhysChem **11**(5), 963–970 (2010).
[81] E. P. Bernard and W. Krauth, "Two-step melting in two dimensions: First-order liquid-hexatic transition," Phys. Rev. Lett. **107**(15), 155704 (2011).
[82] S. C. Kapfer and W. Krauth, "Two-dimensional melting: From liquid-hexatic coexistence to continuous transitions," Phys. Rev. Lett. **114**, 035702 (2015).
[83] B. I. Halperin and D. R. Nelson, "Theory of two-dimensional melting," Phys. Rev. Lett. **41**(2), 121 (1978).
[84] X. Ma, J. Pausch, and M. E. Cates, "Theory of hyperuniformity at the absorbing state transition," arXiv:2310.17391 (2023).
[85] T. Song and H. Xia, "Kinetic roughening and nontrivial scaling in the Kardar–Parisi–Zhang growth with long-range temporal correlations," J. Stat. Mech.: Theory Exp. **2021**(7), 073203.
[86] E. Medina, T. Hwa, M. Kardar, and Y.-C. Zhang, "Burgers equation with correlated noise: Renormalization-group analysis and applications to directed polymers and interface growth," Phys. Rev. A **39**(6), 3053 (1989).
[87] G. Grinstein, D.-H. Lee, and S. Sachdev, "Conservation laws, anisotropy, and 'self-organized criticality' in noisy nonequilibrium systems," Phys. Rev. Lett. **64**(16), 1927 (1990).
[88] P. L. Garrido, J. L. Lebowitz, C. Maes, and H. Spohn, "Long-range correlations for conservative dynamics," Phys. Rev. A **42**(4), 1954 (1990).
[89] R. Aditi Simha and S. Ramaswamy, "Hydrodynamic fluctuations and instabilities in ordered suspensions of self-propelled particles," Phys. Rev. Lett. **89**(5), 058101 (2002).
[90] A. Kundu, O. Hirschberg, and D. Mukamel, "Long range correlations in stochastic transport with energy and momentum conservation," J. Stat. Mech.: Theory Exp. **2016**(3), 033108.
[91] H. Spohn, "Long range correlations for stochastic lattice gases in a non-equilibrium steady state," J. Phys. A: Math. Gen. **16**(18), 4275 (1983).
[92] J. R. Dorfman, T. R. Kirkpatrick, and J. V. Sengers, "Generic long-range correlations in molecular fluids," Annu. Rev. Phys. Chem. **45**(1), 213–239 (1994).
[93] G. Grinstein, "Generic scale invariance in classical nonequilibrium systems (invited)," J. Appl. Phys. **69**(8), 5441–5446 (1991).

[94]P. Bak, "Self-organized criticality in non-conservative models," Physica A **191**(1–4), 41–46 (1992).
[95]J. A. Bonachela and M. A. Munoz, "Self-organization without conservation: True or just apparent scale-invariance?," J. Stat. Mech.: Theory Exp. **2009**(09), P09009.
[96]R. L. Jack, I. R. Thompson, and P. Sollich, "Hyperuniformity and phase separation in biased ensembles of trajectories for diffusive systems," Phys. Rev. Lett. **114**(6), 060601 (2015).
[97]L. Caprini, U. Marini Bettolo Marconi, A. Puglisi, and H. Löwen, "Entropons as collective excitations in active solids," J. Chem. Phys. **159**(4), 041102 (2023).
[98]M. Huang, W. Hu, S. Yang, Q.-X. Liu, and H. P. Zhang, "Circular swimming motility and disordered hyperuniform state in an algae system," Proc. Natl. Acad. Sci. U. S. A. **118**(18), e2100493118 (2021).
[99]B. Zhang and A. Snezhko, "Hyperuniform active chiral fluids with tunable internal structure," Phys. Rev. Lett. **128**(21), 218002 (2022).
[100]Z. Ma and S. Torquato, "Random scalar fields and hyperuniformity," J. Appl. Phys. **121**(24), 244904 (2017).
[101]S. Wilken, A. Chaderjian, and O. A. Saleh, "Spatial organization of phase-separated DNA droplets," Phys. Rev. X **13**(3), 031014 (2023).
[102]Y. Zheng, M. A. Klatt, and H. Löwen, "Universal hyperuniformity in active field theories," arXiv:2310.03107 (2023).
[103]F. De Luca, X. Ma, C. Nardini, and M. E. Cates, "Hyperuniformity in phase ordering: The roles of activity, noise, and non-constant mobility," J. Phys.: Condens. Matter **36**, 405101 (2024).
[104]L. Corte, P. M. Chaikin, J. P. Gollub, and D. J. Pine, "Random organization in periodically driven systems," Nat. Phys. **4**(5), 420–424 (2008).
[105]D. J. Pine, J. P. Gollub, J. F. Brady, and A. M. Leshansky, "Chaos and threshold for irreversibility in sheared suspensions," Nature **438**(7070), 997–1000 (2005).
[106]R. Brito, D. Risso, and R. Soto, "Hydrodynamic modes in a confined granular fluid," Phys. Rev. E **87**(2), 022209 (2013).
[107]A. Plati, R. Maire, E. Fayen, F. Boulogne, F. Restagno, F. Smallenburg, and G. Foffi, "Quasi-crystalline order in vibrating granular matter," Nat. Phys. **20**, 465 (2024).
[108]F. Smallenburg, "Efficient event-driven simulations of hard spheres," Eur. Phys. J. E **45**(3), 22 (2022).
[109]J. Javier Brey, V. Buzón, P. Maynar, and M. I. García de Soria, "Hydrodynamics for a model of a confined quasi-two-dimensional granular gas," Phys. Rev. E **91**(5), 052201 (2015).
[110]V. Garzó, R. Brito, and R. Soto, "Enskog kinetic theory for a model of a confined quasi-two-dimensional granular fluid," Phys. Rev. E **98**(5), 052904 (2018).
[111]Y. Komatsu and H. Tanaka, "Roles of energy dissipation in a liquid-solid transition of out-of-equilibrium systems," Phys. Rev. X **5**(3), 031025 (2015).
[112]K. J. Runge and G. V. Chester, "Monte Carlo determination of the elastic constants of the hard-sphere solid," Phys. Rev. A **36**(10), 4852 (1987).
[113]D. Frenkel and A. J. C. Ladd, "Elastic constants of hard-sphere crystals," Phys. Rev. Lett. **59**(10), 1169 (1987).
[114]B. B. Laird, "Weighted-density-functional theory calculation of elastic constants for face-centered-cubic and body-centered-cubic hard-sphere crystals," J. Chem. Phys. **97**(4), 2699–2704 (1992).
[115]F. V. Reyes and J. S. Urbach, "Effect of inelasticity on the phase transitions of a thin vibrated granular layer," Phys. Rev. E **78**(5), 051301 (2008).
[116]J. S. Olafsen and J. S. Urbach, "Clustering, order, and collapse in a driven granular monolayer," Phys. Rev. Lett. **81**, 4369–4372 (1998).
[117]W. Losert, D. G. W. Cooper, and J. P. Gollub, "Propagating front in an excited granular layer," Phys. Rev. E **59**, 5855–5861 (1999).
[118]A. Prevost, P. Melby, D. A. Egolf, and J. S. Urbach, "Nonequilibrium two-phase coexistence in a confined granular layer," Phys. Rev. E **70**, 050301 (2004).
[119]B. Néel, I. Rondini, A. Turzillo, N. Mujica, and R. Soto, "Dynamics of a first-order transition to an absorbing state," Phys. Rev. E **89**(4), 042206 (2014).
[120]M. Argentina, M. G. Clerc, and R. Soto, "van der Waals–like transition in fluidized granular matter," Phys. Rev. Lett. **89**, 044301 (2002).
[121]M. G. Clerc, P. Cordero, J. Dunstan, K. Huff, N. Mujica, D. Risso, and G. Varas, "Liquid–solid-like transition in quasi-one-dimensional driven granular media," Nat. Phys. **4**(3), 249–254 (2008).
[122]G. Castillo, N. Mujica, N. Sepúlveda, J. C. Sobarzo, M. Guzmán, and R. Soto, "Hyperuniform states generated by a critical friction field," Phys. Rev. E **100**(3), 032902 (2019).
[123]L. Lovász, "Discrete and continuous: Two sides of the same?," in *Visions in Mathematics: GAFA 2000 Special Volume, Part I* (Springer, 2010), pp. 359–382.
[124]J. L. Gross, J. Yellen, and M. Anderson, *Graph Theory and its Applications* (Chapman and Hall/CRC, 2018).
[125]A. Cavagna, J. Cristín, I. Giardina, T. S. Grigera, and M. Veca, "Discrete Laplacian thermostat for flocks and swarms: The fully conserved Inertial Spin Model," arXiv:2403.07644 (2024).
[126]A. Cavagna, J. Cristín, I. Giardina, and M. Veca, "Discrete laplacian thermostat for spin systems with conserved dynamics," Phys. Rev. B **107**, 224302 (2023).
[127]K. H. Michel, S. Costamagna, and F. M. Peeters, "Theory of anharmonic phonons in two-dimensional crystals," Phys. Rev. B **91**(13), 134302 (2015).
[128]M. D. Bustamante, K. Hutchinson, Y. V. Lvov, and M. Onorato, "Exact discrete resonances in the Fermi-Pasta-Ulam-Tsingou system," Commun. Nonlinear Sci. Numer. Simul. **73**, 437–471 (2019).
[129]S. Nazarenko, *Wave Turbulence* (Springer Science & Business Media, 2011), Vol. 825.
[130]T. Harada and S.-i. Sasa, "Equality connecting energy dissipation with a violation of the fluctuation-response relation," Phys. Rev. Lett. **95**(13), 130602 (2005).
[131]A. Crisanti, A. Puglisi, and D. Villamaina, "Nonequilibrium and information: The role of cross correlations," Phys. Rev. E **85**(6), 061127 (2012).
[132]J. S. Lee and H. Park, "Stochastic thermodynamics and hierarchy of fluctuation theorems with multiple reservoirs," New J. Phys. **20**(8), 083010 (2018).
[133]Y. Murashita and M. Esposito, "Overdamped stochastic thermodynamics with multiple reservoirs," Phys. Rev. E **94**(6), 062148 (2016).
[134]C. Van den Broeck and M. Esposito, "Three faces of the second law. II. Fokker-Planck formulation," Phys. Rev. E **82**(1), 011144 (2010).
[135]A. Puglisi, P. Visco, E. Trizac, and F. van Wijland, "Dynamics of a tracer granular particle as a nonequilibrium Markov process," Phys. Rev. E **73**(2), 021301 (2006).
[136]A. Sarracino, D. Villamaina, G. Costantini, and A. Puglisi, "Granular brownian motion," J. Stat. Mech.: Theory Exp. **2010**(04), P04013.
[137]A. Plati, A. Puglisi, and A. Sarracino, "Thermodynamic bounds for diffusion in nonequilibrium systems with multiple timescales," Phys. Rev. E **107**(4), 044132 (2023).
[138]A. Plati and A. Puglisi, "Slow time scales in a dense vibrofluidized granular material," Phys. Rev. E **102**, 012908 (2020).
[139]N. E. Glatt-Holtz, D. P. Herzog, S. A. McKinley, and H. D. Nguyen, "The generalized Langevin equation with power-law memory in a nonlinear potential well," Nonlinearity **33**(6), 2820 (2020).
[140]G. A. Pavliotis, *Stochastic Processes and Applications* (Springer, 2016).
[141]I. Goychuk, "Viscoelastic subdiffusion: From anomalous to normal," Phys. Rev. E **80**(4), 046125 (2009).
[142]R. Kupferman, "Fractional kinetics in Kac–Zwanzig heat bath models," J. Stat. Phys. **114**, 291–326 (2004).
[143]M. M. Dygas, B. J. Matkowsky, and Z. Schuss, "A singular perturbation approach to non-Markovian escape rate problems with state dependent friction," J. Chem. Phys. **84**(7), 3731–3738 (1986).
[144]A. Puglisi and D. Villamaina, "Irreversible effects of memory," Europhys. Lett. **88**(3), 30004 (2009).
[145]L. Ma, X. Li, and C. Liu, "Fluctuation-dissipation theorem consistent approximation of the Langevin dynamics model," Commun. Math. Sci. **15**(4), 1171–1181 (2017).
[146]I. Pagonabarraga, E. Trizac, T. P. C. van Noije, and M. H. Ernst, "Randomly driven granular fluids: Collisional statistics and short scale structure," Phys. Rev. E **65**(1), 011303 (2001).